UNIVERITY OF LATVIA RIGA TECHNICAL UNIVERSITY
JOINT ACADEMIC BACHELOR STUDIES PROGRAMM
“BIOTECHNOLOGY AND BIOENGINEERING”

EXPRESSION, PURIFICATION AND CHARACTERIZATION OF AMADORIASE MUTANTS FOR THE DETECTION OF GLYCATED HEMOGLOBIN

BACHELOR THESIS

Author: **Leonid Rozanov**
Stud. apl. Nr. lr21049
Supervisor: Dr. chem. Emilio Parisini

RIGA 2024

ABSTRACT

Fructosyl peptide oxidases, also known as amadoriases, are a class of FAD-dependent enzymes that can find application in diagnostics tests for diabetes. However, owing to some existing limitations to their usability, namely the size of accessions tunnel to their active site, these enzymes must be extensively engineered to allow the development of a cheap and easy-to-use diabetes monitoring device.

The aim of this work is to evaluate the thermostability, the activity and the structural features of two novel amadoriase mutants, D7 and D11, which have been designed based on a mutant (X02C) previously designed and characterized in our group.

To achieve these goals, proteins were produced in *E. coli* cells. The two mutants were then purified using a combination of nickel affinity chromatography and size exclusion chromatography. The thermostability and and secondary structures of the two mutants were analyzed using circular dichroism. Enzymatic assays were performed on the natural substrate, the fructosyl-VH (f-VH) dipeptide, to assess the activity of the enzymes. One of the two enzymes (D7) was crystallized using the vapor diffusion method. The structure was solved by molecular replacement and refined at 2.1 Å resolution. While both mutants showed reduced thermostability and lower expression yield compared to their parent enzyme, their activity on f-VH increased. However, no measurable activity could be detected on larger substrates.

Key words: Amadoriase, FPOX, AGEs, diabetes, deglycation, crystal structure

KOPSAVILKUMS

Fruktozīla peptīdu oksidāzes, ko dēvē arī par amadoriāzēm, ir no FAD atkarīgo enzīmu klase, ko var izmantot diabēta diagnostikas testos. Tomēr, ņemot vērā dažus esošos ierobežojumus to lietojamībai, proti, piekļuves tuneļa lielumu tā aktīvam centram, šie enzīmi ir jāveic dažadās izmaiņas proteīna sekvencē, lai varētu izstrādāt lētu un ērti lietojamu diabēta uzraudzības ierīci.

Šī darba mērķis ir novērtēt divu jaunu amadoriāzes mutantu - D7 un D11- termostabilitāti, aktivitāti un strukturālās iezīmes, kas veidotas, balstoties uz mutanta (X02C), kurš iepriekš bija izstrādāts un raksturots mūsu laboratorijā.

Lai sasniegtu šos mērķus, proteīni tika biosintezēti *E. coli* šūnās. Pēc tam abus mutantus attīrīja, izmantojot niķeļa afinitātes hromatogrāfijas un izmēru izslēgšanas hromatogrāfijas kombināciju. Abu mutantu termostabilitāti un sekundārās struktūras analizēja noteica ar cirkulāro dihroismu. Enzimātiskus testus veica ar dabisko substrātu – fruktosila-VH (f-VH) dipeptīdu, lai novērtētu enzīmu aktivitāti. Viens no diviem enzīmiem (D7) tika kristalizēts, izmantojot tvaiku difūzijas metodi. Struktūra tika atrisināta ar molekulāru nomaiņu un precizēta, ar izšķirtspēju 2.1 Å. Lai gan abiem mutantiem bija mazāka termostabilitāte un mazāks biosintēzes iznākums, salīdzinot ar pamatenzīmu, to aktivitāte uz f-VH palielinājās, tomēr ar lielāku substrātu nebija iespējams noteikt tā aktivitāti.

Atslēgas vārdi: Amadoriāze, FPOX, AGG, diabēts, deglicēšana, kristāla struktūra

TABLE OF CONTENT

LIST OF ABBREVIATIONS

°C– degree Celsius

AGE – advanced glycation endproduct

CD-circular dichroism

EDTA-ethylenediaminetetraacetic acid

FAD-flavin adenine dinucleotide

FAOX- fructosyl amino acid oxidase

FV -fructosyl-valine

FPOX – fructosyl peptide oxidase

HbA1c- hemoglobin A1c

IPTG- isopropyl-beta-D-thiogalactoside

LB- Luria Bertani broth

MD-molecular dynamics

mM-millimolar

RMSF-root mean square fluctuation

SDS- sodium dodecyl sulfate

SDS-PAGE- sodium dodecyl sulfate–polyacrylamide gel electrophoresis

SEC- size exclusion chromatography

UV-ultraviolet

µg– microgram

µl– microliter

µm-micrometer

µmol- micromole

INTRODUCTION

Over the last few decades, diabetes has become one of the fastest growing health complications in the human population. According to the International Diabetes Association, it has been estimated that the number of patients with this illness in 2021 was around 537 million (International Diabetes Association, 2024). As this number is expected to rise to 783 million by 2045, it is urgent to develop effective strategies for fast and reliable diagnosis.

Despite being the least reactive among the common sugars, glucose is capable of glycating proteins via the Maillard reaction. (Martins, et al 2000) This results in the formation of the so-called advanced glycation end products (AGEs), which are amino acid-sugar adducts. Upon formation of an initial Schiff base, these initial adducts eventually undergo rearrangement into Amadori products. The formation of Amadori products negatively impacts the proteins, lowering their ligand binding capabilities and/or their enzymatic activity. Interestingly, glycation results in the formation glycated hemoglobin, one of the main diabetes markers.

Using naturally deglycating enzymes such as amadoriases to target Amadori products is a promising strategy to reduce AGEs formation. Fructosyl peptide oxidases (FPOX), are members of the amadoriase family of enzymes also known as FAOX (fructosyl amino acid oxidases). As such enzymes are capable of catalyzing the deglycation of amino acids, they could be used to prevent, or revert, Amadori product formation. These FAD-dependent enzymes, which are members of the oxidoreductase family, have been studied as potential tools for diabetes detection, as well as food production processes. The main limitations of this class of enzymes is its inability to act on high molecular weight substrates and inactivity on whole proteins.

Hypothesis: Engineering of Amadoriase enzymes may lead to an enhanced activity towards larger substrates such as intact glycated proteins

Aim of the study: To assess the thermal stability and the enzymatic activity of a number of novel computationally designed FPOX mutants.

Established tasks:

- To successfully express and purify enzymes produced by molecular dynamic simulations.
- To assess the stability of the mutants via biophysical assays.
- To crystallize mutants and produce at least crystal structure in order to asses, if our goal of enlarging the active site is achieved

This thesis is part of a larger study conducted in the Biotechnology group led by Dr. Emilio Parisini at the Latvian Institute of Organic Synthesis (Riga, Latvia)

LITERATURE REVIEW

1.1 Protein glycation

There are two major protein modifications that occur due to the presence of carbohydrates – glycation and glycosylation. Glycosylation involves glycosyltransferases, which are enzymes involved in the synthesis of carbohydrate units of proteins. The most common types of glycosylation are N-linked and O-linked glycosylation. While N-linked glycosylation refers to the formation of a link between a sugar and an asparagine (N) residue, O-linked glycosylation occurs between a sugar and a serine or threonine (O) residue. Glycation, on the other hand, is a spontaneous non-enzymatic reaction between a protein and a reducing sugar that occurs at random locations on proteins, resulting in the formation of so-called advanced glycation end products (AGEs). (Andreas *et al* 2011)

Glycation was first described by the French chemist L.C. Maillard in the early 20th century. In his work, Maillard described the reaction between amino acids and carbohydrates (the so-called "Maillard reaction"). This is a spontaneous non-enzymatic reaction that occurs between a protein and a reducing sugar and results in the formation of brown pigments and protein-protein crosslinks. This reaction, which is very widespread, commonly occurs during food preparation, especially at elevated temperatures, as well as during the manufacturing processes of textiles and paper. One of the most common components of the Maillard reaction is glucose. Despite being the least active among the common sugars, glucose is capable of reacting with nucleophilic nitrogen bases of proteins, such as the tertiary amine of lysines and arginines, resulting in the initial formation of a Schiff base. (Ulrich *et al* 2001) Following rearrangement into fructosylamines, these adducts further transform into advanced glycation end products, which are capable of cross-linking amino acids in proteins (Fig. 1). AGEs accumulation in the body is commonly associated with adverse health complications due to the fact that these cross-linking reactions are irreversible. (Prasad *et al* 2017) Among the most common health complication associated with diabetes and AGEs formation are arterial stiffening, nephropathy, retinopathy and the onset of Alzheimer's disease and Parkinson's disease.

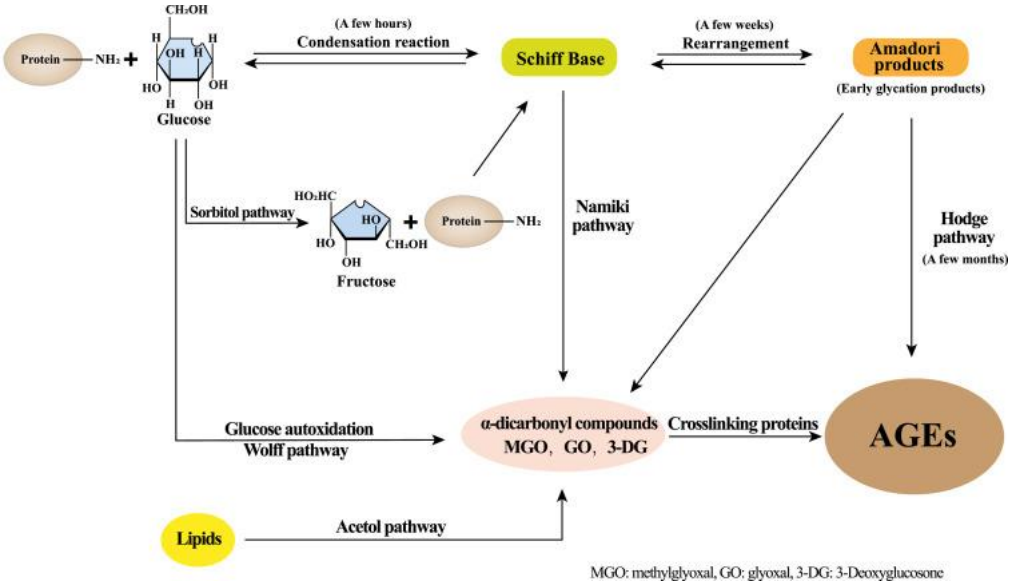

Fig 1. Formation of Advanced glycation end products.

Reaction between a protein and glucose produces a Schiff base. Shiff bases undergo rearrangement to Amadori products which are then converted into AGEs (adapted from Quinge S. *et al*. 2021)

Att 1. Advancēto glicēto galaproductu izveide.

Reakcija starp proteīnu un glikozi rada *Šifa* bāzi. *Šifa* bāzes tiek pārveidotas par Amadori produktiem, kuri pēc tam tiek konvertēti par AGG (aizgūts no Quinge S. *et al.* 2021)

1.2 Exogenous AGEs

Besides forming spontaneously in the body, AGEs can also be accumulated via dietary intake of cooked or heavily processed foods. Certain cooking conditions such as high temperatures for prolonged periods of time, low hydration levels and high pH generate large amounts of AGEs. It is speculated that most of the exogenous AGEs that accumulate in the body come with the intake of certain foods and beverages and it has been estimated that daily intake of advanced glycation end products should not exceed 75 mg. (Mastrocola *et al* 2020) Although exogenous and endogenous AGEs show much biological similarity, endogenous AGEs possess much higher health risks. (Rungratanawanich *et al* 2021)

While it is estimated that around 10% of ingested AGEs are absorbed into tissues through meals, approximately two thirds are accumulated and later exhibit pathological effects. (Zhang *et al* 2023) Another aspect that makes them dangerous is the fact that AGEs cannot be secreted with urine, leading to their accumulation in the tissues. (Chaudhuri *et al* 2018)

Despite the demonstrated effectiveness of dietary changes on AGEs-related health

complications, which lead to a reduction of oxidative stress and inflammation, it is still not known to what extent dietary AGEs contribute to the overall pool (Mastrocola *et al* 2020)

1.3 Endogenous AGEs

Endogenous advanced glycation end products keep forming throughout the entire life. They are formed via a non-enzymatic reaction between sugar and long-lived endogenous proteins. These reactions are enhanced by the presence of oxidative stress or hyperglycemia, or simply occur as a result of aging. (Zeng et al 2019) Glycation usually occurs on residues carrying tertiary amines like arginine or lysine; however, histidine, tryptophan or cysteine can also be affected. As glycation directly influences the structure of biological molecules, such modifications result in a lower quality of long-lived proteins as well as in a reduction in their bioavailability. (Nowotny *et al* 2018) Due to the involvement of various precursors (such as, for instance, dicarbonyls), glycation end products are formed as heterogeneous compounds with varying molecular mass.

1.4 Pathological effects of AGEs

AGEs formation is a process that affects all individuals. Certain population groups, however, such as the elderly and type 2 diabetes patients are impacted the most. The harmful effects of the accumulation of endogenous AGEs cause changes in enzymatic activity and ligand binding across a wide range of proteins, particularly in, but not limited to, long-lived proteins. (Nessar et al 2005). Another harmful effect of AGEs is the glycation of lipoproteins, low density lipoproteins and lipids. Such changes are most prevalent in patients with type 2 diabetes, as shown by the high levels of low-density lipoproteins that accumulate in their blood, which can increase the risks of coronary heart disease and stroke. (Vekic *et al* 2023)

Over time even modest level of hypoglycemia can cause significant accumulation of AGEs, particularly on hemoglobin, albumin and other long-lived proteins. (Vlassara *et al* 2002)

Oxidative stress is commonly associated with neurodegenerative disorders such as Alzheimer's, Huntington's, or Creutzfeldt-Jakob. A common symptom of these ailments is a decline in neural signal transmission, which is also associated with neural loss. Another similarity shared by these disorders is an accumulation of AGEs in the brain. In this case, the presence of AGEs induces the production of amyloid precursor protein, thus facilitating accumulation of amyloid β in the brain. Hence, the presence of AGEs can be a trigger in the development the of Alzheimer's disease. Indeed, AGEs can be detected in pathological deposits

such as neurofibrillary tangles or amyloid plaques. Furthermore, the accumulation of AGEs promotes the generation of protease-resistant products which results in an impaired supply of cholesterol and fat to neurons. (Nedić *et al* 2013)

1.5 Glycation of hemoglobin

Hemoglobin is a gas transporting protein that is capable of carrying oxygen from the lungs to the other tissues in mammals. Hemoglobin's affinity for oxygen allows an almost complete saturation of the protein with the gas, resulting in a highly efficient transport throughout the body. (Kaushansky *et al* 2021) With a half-life of around 120 days, hemoglobin is considered a long-lived protein and, as such, it is highly susceptible to glycation. (Troester *et al* 2000) HbA1c is the most abundant form of glycated hemoglobin. In HbA1c, the N-terminal valine of hemoglobin reacts with glucose, resulting in their non-enzymatic attachment via Shiff base formation. (Sen *et al* 2005)

Unlike direct glucose measurement, which indicates the concentration of glucose in the blood at the time of the analysis, HbA1cmeasurement provides an accurate representation of glucose concentration over time and allows a more reliable monitoring of sugar levels in the blood. Indeed, is important to stress that this measurement reflects the blood glucose concentration over the previous four to eight weeks. Other long-lived proteins such as albumin, with half-life of 20 days, (Haque et al 2013) and skin collagen, with half- life of 15 years ,(Verzijl *et al* 2000) can also undergo such changes. As already mentioned these modifications result in loss of function and pathological outcomes. (Rondeau *et al* 2011)

1.6 Amadoriases

Amadoriases or fructosyl amine oxidases (FAOX) are FAD-dependent enzymes that belong to the oxydoreductase family and are commonly found in yeast, fungi and bacteria. These enzymes have an ability to cleave low molecular weight Amadori products via a reaction that results in the formation of a free amine, glucosone and hydrogen peroxide (Fig.2).

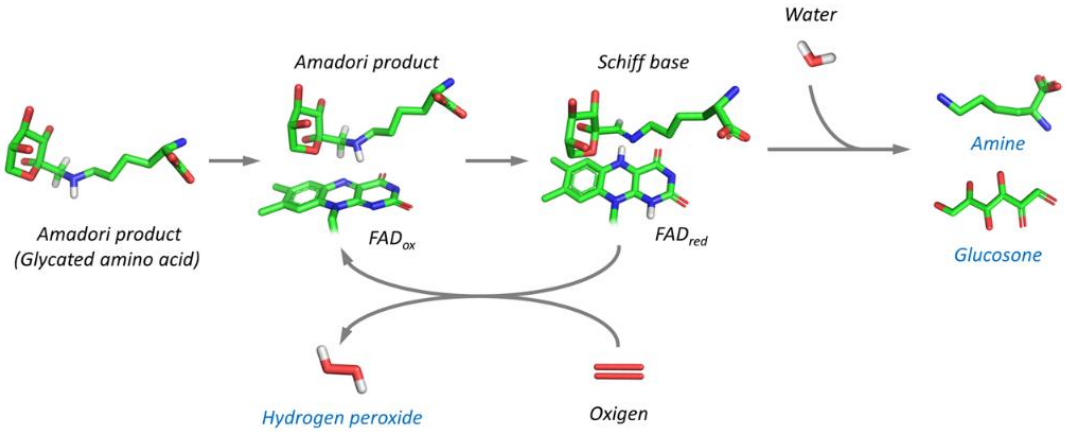

Fig 2. Reaction between an Amadori product and Amadoriase

Att 2. Reakcija starp Amadori produktu un Amadoriāzi

Due to their substrate specificity, amadoriases have been categorized into three groups. Group 1 is mostly active on α-fructosyl amino acids (Fig. 3), group 2 is active on ε-fructosyl amino acids while group 3 show similar activity both on α-fructosyl amino acids and ε-fructosyl amino acids. (Rigoldi *et al* 2016)

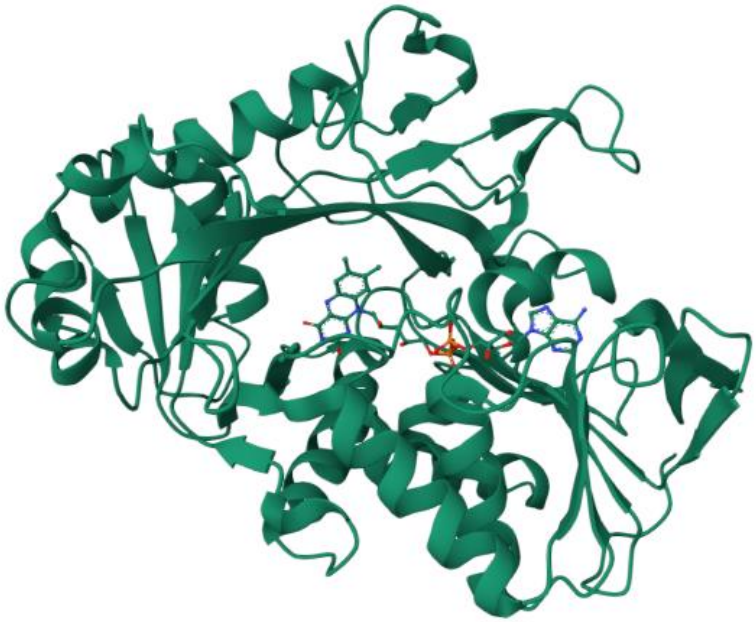

Fig 3. Crystal structure of Amadoriase I from *Aspergillus fumigatus* (PDB: 4WCT). (adapted from Rigoldi F. *et al*.2016)

Att 3. Amadoriāzes I kristāla struktūra no *Aspergillus fumigatus* (PDB: 4WCT).

Amadoriases are viewed as a promising tool for the measurement of glycated hemoglobin (HbA1C) in the blood. The most important aspect of such assays is the detection of the glycated N-terminal valine of Hb1AC. However, due to the limited size of their active site, FPOXs are inactive on intact Hb1AC. Therefore, the assays require an additional step, a preliminary proteolytic digestion, in order to release the N-terminal valine residue (Fig. 4). This step increases the time and the resources that are needed to perform the assay.

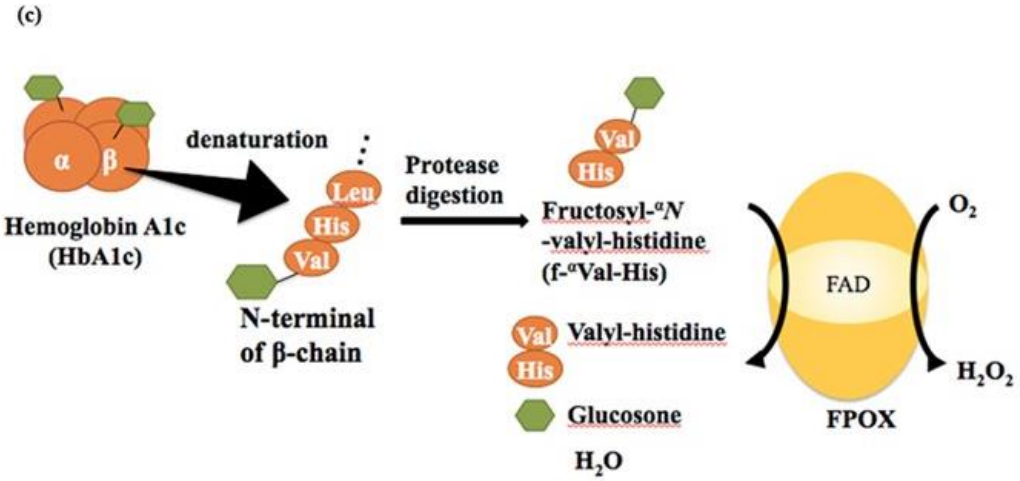

Fig 4. Scheme of Hb1AC detection assay (adapted from Shimasaki T. et al. 2017)

Att 4. Hb1AC noteikšanas testa shēma (aizgūts no Shimasaki T. et al. 2017)

1.7 Fructosyl peptide oxidases (FPOX)

Fructosyl peptide oxidase are part of the FAOX family. Currently, these enzymes are used for the detection of HbA1c, which is a long-term diabetes marker. Kits that utilize these enzymes are based on the preliminary proteolytic digestion of HbA1c, which results in a release of various amino acids, including the N-terminal glycation-prone valine. Upon processing the glycated valine substrate, FPOX releases hydrogen peroxide which can be measured via a colorimetric assay that involves the use of horseradish peroxidase as a chromophore.

Our group has long been working on the engineering of FPOX with the goal of enlarging the accession tunnel to the active site of the enzyme in order to allow the use of this class of enzymes on intact proteins. At the engineering level, this requires both an enlargement of the accession tunnel to the active site of the enzyme and a stabilization of the mutated enzyme, to compensate for the removal of parts of the original structure. In general, engineered enzymes benefit greatly from thermal stabilization, to compensate for the removal of some structurally important portions. Moreover, biological components of detection kits usually require enhanced

stability for long-term storage, which is an absolute requisite for their successful commercialization.

In order to meet these requirements, various stabilization methods have been attempted in the past. In our group, we have always taken a rational design approach to protein stabilization, introducing various changes to the sequence. For instance, the introduction of various disulfide bonds through site – directed mutagenesis was proven to be an effective strategy to increase thermostability. Clearly, the location in which such mutations are introduced play an important role for achieving the expected result. For instance, one of the mutants with mutations H106C and G150C was shown to feature a decreased activity due to the mutations being too close to substrate tunnel. However, in a previous round of engineering one of the designed mutants (the so-called SS17 mutant) featuring the mutations D295C and K303C was shown to display a significant improvement in thermostability (from 52.4 to 60.6°C) without losing any specific activity towards its natural substrate. Indeed, the electron density map determined by X-ray crystallography showed clear disulfide bond formation in the position where double cysteine mutation was introduced (Fig. 5). (Rigoldi *et al* 2018)

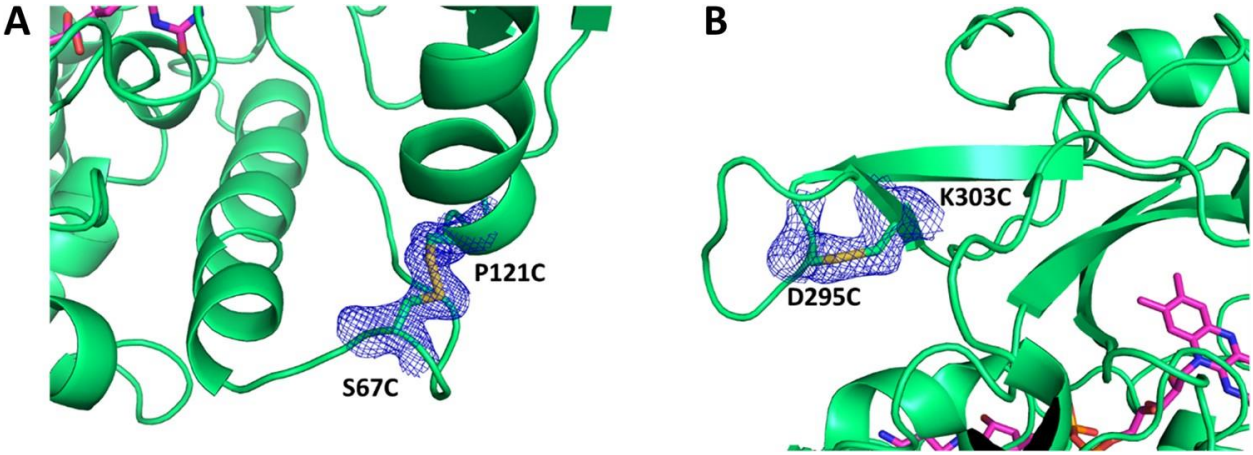

Fig 5. Electron density maps of the double cysteine mutation.

Detailed view of double cysteine mutation of the SS03 mutant (panel A, PDB: 5OC3) and SS17 mutant (panel B, PDB: 5OC2) (adapted from Rigoldi *et al* 2018)

Att 5. Dubulto cisteīnu mutāciju elektronu blīvuma kartes

Detalizēts pārskats ar dubulto cisteīna mutāciju SS03 mutantam (A panelis, PDB 5OC3) un SS17 mutantam (B panelis, PDB: 5OC2) (aizgūts no Rigoldi *et al* 2018)

Subsequent rounds of engineering that were previously done in our group were directed toward the shortening of one of the two alpha helices (helix III, Fig. 6) that act as gating structures to the catalytic pocket and the shortening of the loop that connects it to the rest of the

structure. This led to a mutant (X02C) that featured good activity also toward larger substrates such as the N-teminal glycated hexapeptide of HbA1c.

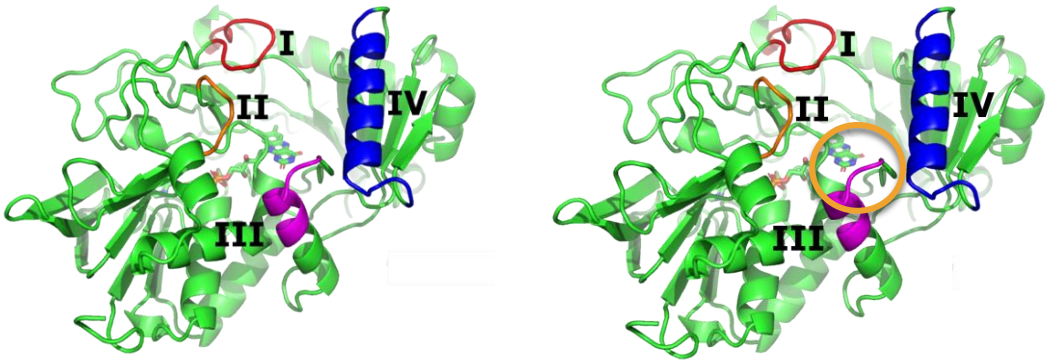

Fig. 6. Crystal structure of FPOX showing: A) the two alpha helices that act as gating structures to the active site of the enzyme. B) In the circle, the portion of helix II that was removed in a previous round of engineering and the connecting loop that was also shortened in the process, leading to the stable and active X02C mutant. Both elements are shown in magenta.

Att. 6. FPOX kristāla struktūra, kas rāda: A) divas alfa spirāles, kas darbojas kā enzīma aktīvās vietas strobēšanas struktūras. B) Aplī – spirāles II daļa, kas tika noņemta iepriekšējā inženierijas kārtā, un savienojošā cilpa, kas arī tika saīsināta procesā, radot stabilu un aktīvu X02C mutantu. Abi elementi ir parādīti magenta krāsā.

Among the four different gating structures to the catalytic pocket, we must also count loop I and loop II. However, while these two loops appear to create some impediment to the access of larger substrates to the catalytic pocket, they carry some amino acids that are crucial for the catalytic activity of the enzyme. As such, we are not introducing any modifications to these two loops. Rather, in our group we are currently working toward the removal of a portion of helix IV, one of the remaining gating structures that block access to the catalytic pocket of the enzyme. In particular, we have designed and selected a number of mutants where helix IV has been shortened by one turn and the loop connecting it to the adjacent beta strand has been remodeled (Fig. 7).

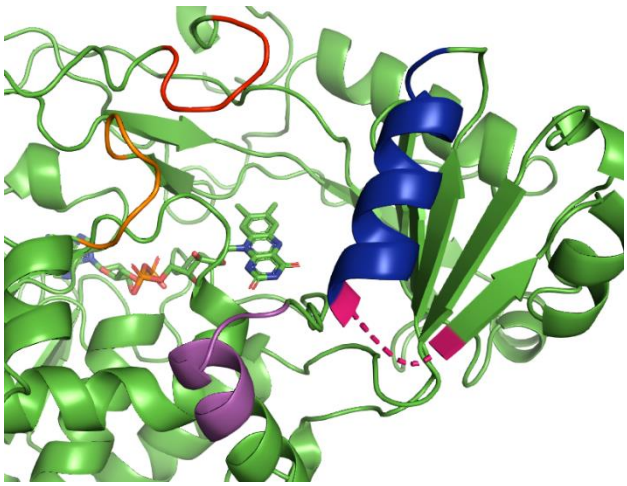

Fig. 7. The current round of engineering is focusing on the shortening of helix IV, one of the secondary structure elements that blocks the access of large substrates to the catalytic pocket. Helix IV is shown in blue, while the remodeled portion is shown in pink.

Att. 7. Pašreizējā inženierzinātņu kārta ir vērsta uz spirāles IV saīsināšanu, kas ir viens no sekundārās struktūras elementiem, kas bloķē lielu substrātu nonākšanu katalītiskajā kabatā. Helix IV ir zilā krāsā, bet noņemtā daļa ir rozā krāsā.

In this thesis, I describe the work I have done towards the production and the testing of a further set of mutants (D7 and D11) generated via the shortening of alpha helix IV (Fig. 6). Additional mutants from this round of engineered have been studied by other members of the group and will not be described here as the work is still largely ongoing.

MATERIALS AND METHODS

2.1.1Materials

Table 1. Materials

1.tabula. Materiāli

Apparatus	Model	Manufacturer
Autoclave	DX-65	Systec, Germany
Centrifuge	Avanti J-E	BeckmanCoulter,USA
Centrifuge	AllegraX-30R	BeckmanCoulter,USA
Centrifuge	Microfuge 16	BeckmanCoulter,USA
Centrifuge	Centrifuge 5417R	Eppenfdorf, Germany
Chromatograph	AKTA Pure	Cytiva,Germany
Laboratory scales	SAM_1114_07	Sartorius,Germany
Laminar	HeraSafe	ThermoElectron Corporation,USA
Laminar	Exploris	Köttermann
Thermostat with shaker	Multitron Standard	Infors HT, Switzerland
Spectrophotometer	NanoDrop, Nc	Thermo Fisher Scientific, USA
Vortex	Genie 2	Scientific Industries, USA
-80 freezer	DW-86L579BP	Salvum Ultimate, China
Waterbath	Precision GP 10	Thermo Fisher Scientific, ASV
Sonicator	UP200Ht	Hielscher, Germany
Electrophoresis power supply unit	PowerPac Basic	BioRad,USA
Transluminator for SDS electrophoresis	UVP Visi-White Transilluminator	Analytik Jena,Germany
Microplate reader	Spark 10M	Tecan, Switzerland
Real-Time PCR System	7500Real Time PCR System	AppliedBiosystems, USA
Circular Dichroism Spectrophotometer	J-1500 CD Spectrometer	Jasco, Japan
Ph meter	SevenCompact	MettlerToledo, USA
Stereo microscope	Leica M165 C	Germany
Ultrapure water dispencer	Q-Pod	Millipore, USA

2.1.2 Reagents

Table 2. Reagents

2.tabula. Reagenti

Reagent	Manufacturer	Country
Agar	Carl Roth	France
Ampicillin	Roth Selection	France
FAD	Alfa Aesar	USA
Imidazole	Roth Selection	France
IPTG	Alfa Aesar	USA
Sodium hydroxide	Sigma-Aldrich	USA
Sodium chloride	Roth Selection	France
Tris base	Alfa Aesar	USA
HEPES	Roth Selection	France
CHES	FluoroChem	UK
Polyethelene glycol 20k	Sigma-Aldrich	USA
Polyethelene glycol 8k	Sigma-Aldrich	USA
Polyethelene glycol 6k	Sigma-Aldrich	USA
Polyethelene glycol 4k	Sigma-Aldrich	USA
Glycerol	Alfa Aesar	USA
O-phenylenediamine	Alfa Aesar	USA
Fructosyl-valine	Peptide institute inc	Japan
Fcructose-6-phosphate	Peptide institute inc	Japan
Cryotube	Sarstedt	Germany
HisTrap HP Column, Ni Sepharose High Performance	Cytiva	Germany
HiPrep 26/60 Sephacryl S-100HR	Cytiva	Germany
Amicon™ UltraCentrifugal Filter Units	Merck	USA
96 well plates	Sarstedt	Germany
Quartzquvette	Sigma-Aldrich	USA
22mm siliconezed glass cover slides	Hampton research	USA
24 well crystallization plate	Hampton research	USA

High vacuum grease	Dow Corning	USA

2.1.3 Additional materials

Table 3. Additional materials

3.tabula. Papildu materiāli

Material	Characterization	Manufacturer	Country
Single channel pipette	Research Plus 20-200Ml	Eppendorf International	Germany
	Research Plus 0.1-2.5Ml	Eppendorf International	Germany
	Research Plus 2-20Ml	Eppendorf International	Germany
	Finnpipette 1-10Ml	Thermo Fisher Scientific	USA
	Finnpipette 10-100Ml	Thermo Fisher Scientific	USA
	Finnpipette 1-5ml	Thermo Fisher Scientific	USA
Pipette tips	10,200,1000 Ml	Sarstedt	Germany
Tubes with conical base	1.5, 2, 15, 50 Ml	Sarstedt	Germany
Petri plates	100x20mm	Sarstedt	Germany
Rotilabo stirring magnets bars	15, 20, 25, 30, 40, 50 mm	Roth Selection	France
Crystallograpgy mount	Cryoloop	Hampton research	USA
Magnetic handling tool	CrystalWand Magnetic	Hampton research	USA

2.1.4 Media and buffer solutions

Table 4. Media and buffer solutions

4.tabula. Vides un buferšķīdumi

Ingredients	Quantity
LB Media	
Bacteria Tryptone	10 g/L
Yeast extract	5 g/L
NaCl	10 g/L
pH 7.0 ± 0.2	
Binding buffer	

Tris	50Mm
NaCl	150Mm
Glycerol	5%
Imidazole	20Mm
pH 7.4	
Elution buffer	
Tris	50Mm
NaCl	150Mm
Glycerol	5%
Imidazole	400Mm
pH 7.4	
Size Exclusion buffer / Lysis buffer	
Tris	50Mm
Nacl	150Mm
Glycerol	5%
pH 7.4	
Tris-Glycine	
Tris	0.5M
Glycine	0.5M

2.1.5 Enzymes

Table 5. Enzymes

5.tabula. Enzīmi

Name	Catalog no.	Manufacturer	Country
Protease inhibitor	11836145001	Merck	USA
DNAse	EZ0018	Canvax	Spain

2.1.6 Markers

Table 6. Markers

6.tabula. Markeri

Name	Manufacturer	Country
PageRuler™ Unstained Low Range Protein Ladder	Thermo Fisher Scientific	USA

2.1.7 Bacterial strains and Plasmids

Table 7. Bacterial strains and Plasmids

7. tabula Baktēriju celmi un plazmīdas

Cells	Genotype	Manufecturer, country
SHuffle T7	F´ lac, pro, lacIq / Δ(ara-leu)7697 araD139 fhuA2 lacZ::T7 gene1 Δ(phoA)PvuII phoR ahpC* 21ale (or U) galK λatt::Pneb3-r1-cDsbC (SpecR, lacIq) ΔtrxB rpsL150(StrR) Δgor Δ(malF)3	New England Biolabs, USA
Plasmids		
PET17b	Prokaryotic expression vector	Gene Universal, USA

2.1.8 Software and Algorithms

Table 8. Software and Algorithms

8.tabula Programmatūra un algoritmi

Software	Publisher
CCP4i2	BBSRC
COOT	MRC Laboratory of Molecular Biology
BeStSel	ELTE Eötvös Loránd University

2.2.1 Methods

2.2.2 *E.Coli* transformation

We purchased a pET-17b plasmid carrying the D7 or the D11 gene and we used the heat shock method to transform competent SHuffle cells. Selection of transformed colonies was done using agar plates containing ampicillin.

- Take out Shuffle cells from -80°C freezer. Immediately place cells on ice until thawed
- Add 2 µL of required plasmid, mix gently
- Incubate cells on ice for 30 minutes
- After incubation, give cells a heat shock by placing them in a thermal bath preheated to 42 °C for 45 seconds
- Immediately place cells on ice for 5 minutes
- Add 600 µL of LB to the cells
- Incubate on a shaker for 1 hour at 200 rpm and 37°C
- Centrifuge the cells at 4500 rpm for 5 minutes
- Remove all liquid and resuspend the cell pellet with 100 µL of LB
- Place the cells on LB agar plate containing 100 µg/ml of ampicillin
- Incubate at 37°C for 16 hours

2.2.3 Establishing a glycerol stock

Glycerol stocks allow long term storage of plasmids transformed into the desired bacterial strain at low temperature, eliminating the need of repeating the transformation step. Addition of glycerol is necessary to prevent damage to bacteria and avoiding water crystals. It is recommended to use screw cap tubes as snap top tubes can open unexpectedly during storage.

- After agar plate incubation select a colony
- Using an inoculation tube, transfer it to a culture tube with 10 ml of LB containing 100 µg/ml of ampicillin
- Place in the incubator at 36°C and 200 rpm for 16 hours
- Then pour the culture into a 15 Ml tube and centrifuge at 4500 rpm for 10 minutes
- Remove old media and resuspend the cells in 500 µL of fresh LB
- Place media with the cells into a 2 ml screw cap tube

- Add 500 µL of 50% glycerol and mix by pipetting
- Mark the tube and store at -80°C

2.2.4 Protein production and purification using *E.Coli* expression system and liquid chromatography

Upon obtaining colonies, Shuffle cells were propagated for protein expression and production through large-scale liquid media cultures. For protein purification, we used a combination of immobilized metal-affinity chromatography (IMAC) and size exclusion chromatography (SEC).

- Pick one colony from the agar plate using an inoculation loop.
- Place into a sterile 250 Ml flask and dissolve in 50 ml of LB containing 100 µg/ml of ampicillin
- Incubate for 16 hours at 200 rpm and 37°C
- Centrifuge the overnight culture for 10 minutes at 4500 rpm and 4°C
- Resuspend cells in 4 liters of LB with added ampicillin (100 µg/ml) split this volume in in equal amounts into 6x-2L conical flasks
- Cells are grown on a shaker for 2-4 hours at 200 rpm and 37°C until optical density (OD) reaches OD_{600} = 0.6. Then, temperature is lowered to 18°C and IPTG is added to reach final concentration of 0.1 mM
- Bacteria are cultured overnight on a shaker at 200 rpm and 18°C
- Cells are harvested by centrifugation for 10 minutes at 4500 rpm, 4°C and resuspended in lysis buffer
- Cells are supplemented with FAD, DNAse and PMSF and lysed by sonication on ice
- Sonication is done using the following parameters: “on” time: 15 seconds “off” time: 20 seconds for a total time of 10 minutes.
- Sonicated lysate is then centrifuged at 48000g for 50 minutes at 4°C
- Soluble fraction is then filtered using 0.45 µm filter and run through a HisTrap column prewashed with binding buffer
- Nickel beads are prewashed with binding buffer containing 20 mM imidazole. Then, bound C-terminal His-tagged enzyme is eluted with elution buffer containing 400 mM imidazole

- Eluted protein is loaded into a HiPrep 26/60 Sephacryl S-100 HR size exclusion column pre-equilibrated with SEC buffer
- Best fractions are collected, and their protein concentration is measured using NanoDrop
- Aliquots containing 0.5-1.0 ml of SEC fractions are flash frozen for later use and storage
- Sample purity is analyzed using 12% SDS-PAGE

2.2.5 Protein concentration and cell optical density measurement using NanoDrop spectrometer

NanoDrop spectrometers utilize light from the ultraviolet – visible spectrum to measure protein absorbance. Purified proteins absorb light at 280nm, whilst the most common way to assess microbial growth it to measure optical density at 600nm in a cuvette filled with 1 ml of bacterial culture. The Lambert-Beer law is commonly used to determine the concentration of the sample via absorption. The concentration is determined by using the following equation:

$$c = A / \epsilon L$$

where A is the absorption of the sample, ϵ is an extinction coefficient and L is the path length. Absorption is the intensity of the light passed through sample compared to light before passing, while the extinction coefficient is a measure of the amount of light that the sample absorbs.

- Upon selecting the appropriate operation mode (i.e. OD_{600} measurement for cell optical density and protein A_{280nm} for protein concentration), calibrate the spectrometer by adding 2 µL of buffer directly to emission window when measuring protein concentration or insert a 1ml of LB in a cuvette when measuring cell optical density, click “Blank” and clean detector with clean cloth
- Add 2 µL of sample to emission window or insert a spectroscopy cuvette containing 1ml of media and measure using appropriate mode and parameters.

2.2.6 SDS gel electrophoresis

SDS-PAGE electrophoresis is a way to evaluate the molecular weight of the sample.

When separating proteins though a gel matrix, small proteins move faster due to less resistance. Sodium dodecyl sulfate and polyacrylamide eliminate effects of structure and charge on passing and protein is separated only based on polypeptide chain. An electric field is applied to the sample. This makes negatively charged proteins migrate from negatively charged cathode to positively charged anode.

In this method, there are two gel layers – the stacking gel and the running gel. Stacking layer has a lower percentage of acrylamide and lower pH, which are necessary for accurate sample loading. These factors allow protein to enter the running gel. The running layer has a higher acrylamide content as well as a higher pH. These factors allow samples to separate.

- Preparation of 12% SDS-PAGE gel
- Gather glass plates, combs and a spacer
- Clean the glass and assemble the casting mold
- Pour acrylamide solution for a separating gel and overlay with isopropanol to remove any bubbles and prevent air contact which inhibits polymerization. Allow gels to polymerize for 30 minutes and remove isopropanol.
- Pour acrylamide solution for a stacking gel
- Insert a comb and allow the gel to polymerize
- Wait for 30-40 minutes and, if not used immediately store the gels in the cold room wrapped in moist tissues
- Add 10 μL of ROTI dye to all samples
- Heat the samples at 95°C for 5 minutes.
- Remove the gel from the gel holder.
- Place the gel into the gel electrophoresis apparatus
- Pour 1x Tris – Glycine running buffer into the mount until it overflows and reaches the 1 gel mark
- Load 3 μL of molecular weight marker into the first well, then load 15 μL of samples into the others
- Turn on the power supply, set the machine to 200 V 400 mA and run the gel for 50 minutes or until the ladder fully expands.
- Remove the gel assembly from the machine
- Carefully remove the gel from the glass plates and put it into a shaker box containing dH_2O
- Boil the gel 3 times for 2 minutes, discarding dH_2O after each boil
- Add Coomassie brilliant blue and boil the gel for 2 minutes

- Leave the gel on shaker for 20 minutes
- Discard the dye and boil the gel 3 times for 2 minutes, discarding dH_2O after each boil
- Put gel on lamp to observe results

2.2.6 Crystallization

The hanging drop crystallization method is based on the vapor diffusion method. A 1 µl drop of the protein sample is placed on a cover slip and mished with an identical volume of a crystallizaztion buffer. ! mL of the crystallization buffer is placed into the reservoir against which the hanging drop will be allowed to equilibrate upon sealing the system (Fig. 8).

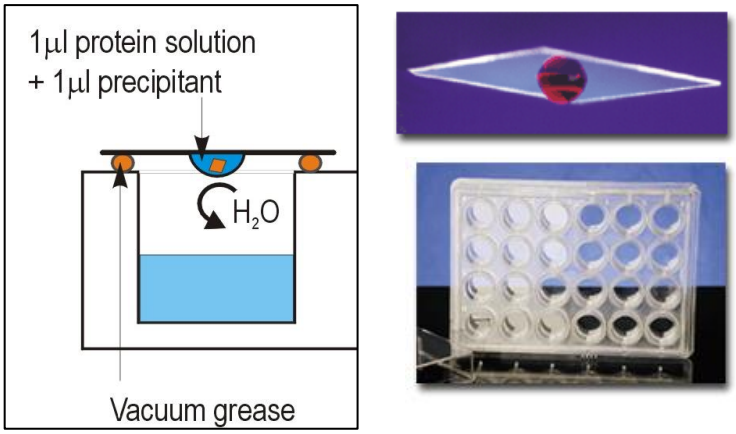

Fig. 8. Schematic representation of a crystallization experiment using the hanging drop technique

Att. 8. Kristalizācijas eksperimenta shematisks attēlojums, izmantojot iekaramā piliena metodi

As the hanging drop features half the concentration of the chemical components that are contained in the reservoir, the drop will start to evaporate as soon as the well is sealed. This will allow the protein content of the hanging drop to concentrate slowly until protein crystals appear.

Calculate the required amounts of reagents for crystallization conditions

- Prepare crystallization conditions by pipetting reagents with combined volume of 1.5 ml into 2 ml tubes

- Prepare a crystallization tray by applying vacuum grease to the rim of each well using a plastic syringe
- Pipet 1 ml of crystallization conditions in each well
- Place 1 µl of protein on a 22mm siliconized glass circle cover slide
- Add 1 µl of crystallization condition to the protein and mix by pipetting up and down
- Seal the well with a cover slide containing the mixture of protein and crystallization condition
- Store in the crystallization room at the constant temperature of 20°C

2.2.7 Circular dichroism

Circular dichroism is based on absorption of left and right circularly polarized light. Due to absorbance of only one type of polarized light by optically active chiral molecules, difference in light absorption can be measured. The UV portion of a circular dichroism spectrum is commonly used to describe aspects of secondary structures of proteins.

- Measurements are performed on JASCO JA-1500 CD spectrometer at 20°C
- Take protein out of -80°C and store on ice until thawed.
- Protein molarity is assessed via the measurement of the absorbance at A280nm using NanoDrop
- Spectra is measured three times using 1-mm pathlength quartz cuvette at protein concentration of 5 µM.
- Upon complete acquisition of the spectrum data are analyzed using the BeStSel spectra analysis method
- Thermal denaturation curves are measured using a capped 2-mm quartz cuvette and a protein concentration of 5 µM.
- Denaturation is induced by heating the sample from 5°C to 95°C at a rate of 1°C/min
- The midpoint of the thermal denaturation process is determined by fitting the data to a curve

2.2.8 Enzymatic assays

Enzymatic activity of the mutants was assessed by measuring the amount of glucosone produced over time in the reaction between the enzymes and natural substrate (fructosyl-valine) at 322nm. The reaction was conducted using a Spark10M plate reader for one hour at 25°C.

- Assay is performed using 96 well transparent polystyrene plate
- 100 µL of sample mixture contain 2mM o-phenylenediamine, 2 mM natural substrate and 10 mM Tris pH 7.4.
- After 1 minute of incubation start the reaction by adding 100 µl the enzyme of interest at the concentration of 1mg/ml
- Increase of absorbance at 322nm (glucosone ε322 = 149.25 M^{-1} cm^{-1}) is monitored using Spark10M at 25°C for one hour
- One unit (U) corresponds to the amount of enzyme required to produce 1 µM of glucosone per minute
- Calculate enzyme activity by dividing moles of product by time
- Calculate specific activity by dividing enzyme activity by the amount of enzyme

2.2.9 Harvesting protein crystals

When crystals are formed, it is necessary to take protein crystals out of the drop in which they have been growing and soak the in a chemically identical solution containing also a certain amount of cryoprotecting agent for low temperature (100 K) data collection at the synchrotron. This way, ice formation is prevented on the surface of the crystals. Moreover, freezing preserves crystals from radiation damage during data collection.

- Prepare cryoprotectant by mixing equal amounts of a 50% glycerol stock solution and the buffer solution corresponding to the condition from the well in which the crystals have formed
- Using a scalpel, carefully open the slip cover to access the drop with crystals
- Transfer 2 µl of cryoprotectant to the drop and mix by pipetting
- Using a pin onto which an appropriate cryo-loop is mounted carefully hook one crystal from the drop
- Transfer the cryo-loop with the sample into a holder placed in liquid nitrogen

- When all the samples are ready, close the cryo-loop holder and transfer it to a shipping dewar chilled with liquid nitrogen

2.2.10 Solving protein structure

Upon obtaining x-ray diffraction data from the synchrotron (DIAMOND light source, Oxford, UK), it was possible to solve the crystal structure. This was done using CCP4i2 suite of programs. Given the high homology of our mutants from the same family that have been preciously structurally characterized, it was possible to solve the structure using the molecular replacement (MR) method. Upon solving the structure, several cycles of structural refinement allowed the modelling of the position of each individual amino acid, hence of the entire structure, and the fit of the calculated electron density map. Correlation between our model and the set of experimental diffraction data is assessed through the R and the R_{free} values.

- Import data obtained from the crystal into CCP4i2
- Create a useable model by importing FASTA file of the mutant and PDB model of XO2B
- Perform a basic molecular replacement using PHASER
- Open COOT and edit the model to correspond to electron density clouds.
- Perform a refinement by importing COOT data into REFMAC5
- After first attempt, re-run the program with suggested parameters.
- Perform several iterative cycles of refinement until R values converge to their lowest possible values.

RESULTS AND DISCUSSION

In this work, I describe two novel FPOX mutants, D7 and D11, which feature a seven-amino acid long reconstruction and the removal of three residues, as well as various other mutations near the engineered position.

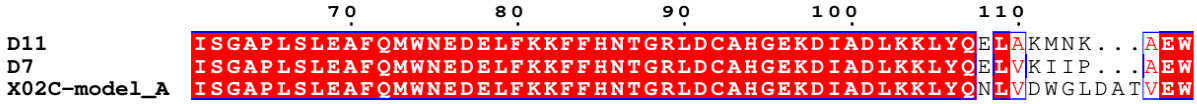

Fig. 9. Portion of the sequence alignment between the mutants and the parent enzyme showcasing the engineered section

Att. 9. Aminoskābju secības salīdzinājums starp mutantiem un pamatenzīmu daļā, kas attēlo konstruēto sekciju

Previously, Estiri and collogues engineered the X02C amadoriase mutant. Here, X02C was used as a basis for another round of rational design aimed at allowing the recognition of larger substrates. I was involved in expression, purification, characterization of two of the engineered mutants as well as in the crystallization experiments and crystal structure solution.

We purchased these mutants into a pET-17b expression vector from Gene Universal. This bacterial vector contains a T7 promoter, which is activated through a lac operon. Hence, it requires IPTG, which is used as a substitute for allolactose, to initiate gene transcription. This plasmid also contains an AmpR gene, which is used a selective marker, as it gives *E. coli* resistance towards the antibiotic ampicillin.

3.1 Gene expression and purification

The two proteins were expressed in SHuffle competent *E. coli* cells. These are cells that are commonly used for expressing protein with disulfide bridges. Cells were transformed and placed on an agar plate containing ampicillin (100µg/ml) as a selection marker (Fig. 10). After incubation, one colony was selected and placed in LB containing 100 µg/ml ampicillin for establishing a large scale (4 liters) culture, as described in the methods section. The protein was purified through combination of immobilized nickel affinity chromatography and size exclusion chromatography and its purity was assessed via gel electrophoresis.

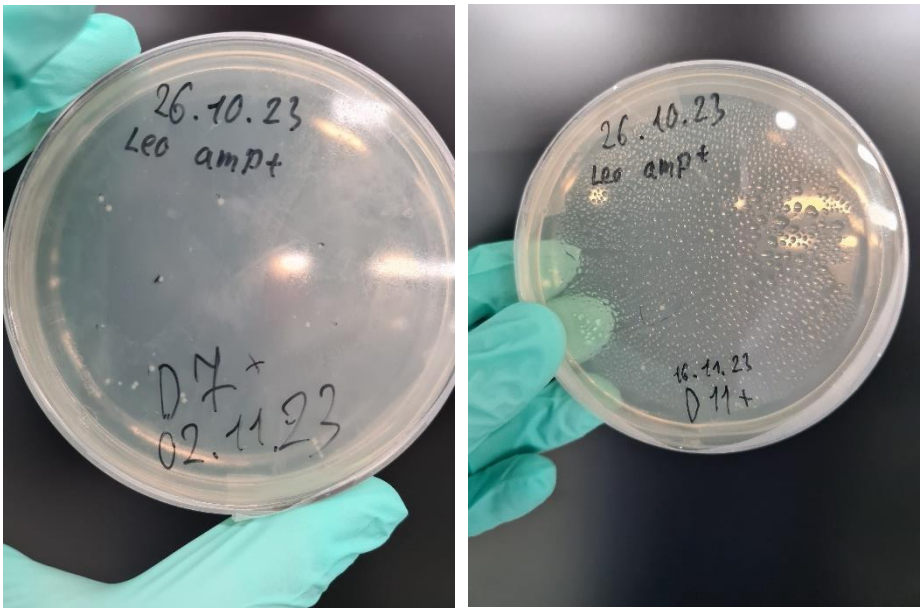

Fig. 10. Agar plates with transformed colonies

Att. 10. Agara plates ar transformētām kolonijām

At first, a 50 ml small scale culture was established. A single colony from either D7 or D11 was added to a flask containing 50 ml of LB plus 100 µg/ml ampicillin and incubated overnight to allow bacterial growth. After overnight incubation, cells were harvested and used for establishing a 4 liter large scale culture. After large scale culture incubation at 37°C until it reached OD_{600} = 0.6, cells were supplemented with IPTG to a final concentration of 0.4 mM and the temperature lowered to 18°C. Cells were later sonicated and purified using ÄKTA pure liquid chromatography system. Effectiveness of the purification was tested via a SDS-PAGE gel electrophoresis. Both mutants showed clear bond at 47kDa after size exclusion chromatography.

Gene expression was followed by two purification steps. Before purification both mutants were supplemented with FAD, DNAse and PMSF. FAD is an Amadoriase cofactor, responsible for correct folding and enzyme activity. FAD gives the protein its characteristic yellow color. DNAse removes all the DNA from the cell lysis, thus lowering the viscosity of the sample for easier elution. PMSF is a protease inhibitor which is necessary for protection of the protein of interest and inactivation of other proteins.

After sonication, samples were purified using nickel affinity chromatography and size exclusion chromatography (Fig. 11 and Fig. 12). Following nickel affinity chromatography, it

was clear that D11 had a higher expression level compared to D7. Both fractions had a distinct yellow color due to a high concentration of protein and to the presence of FAD.

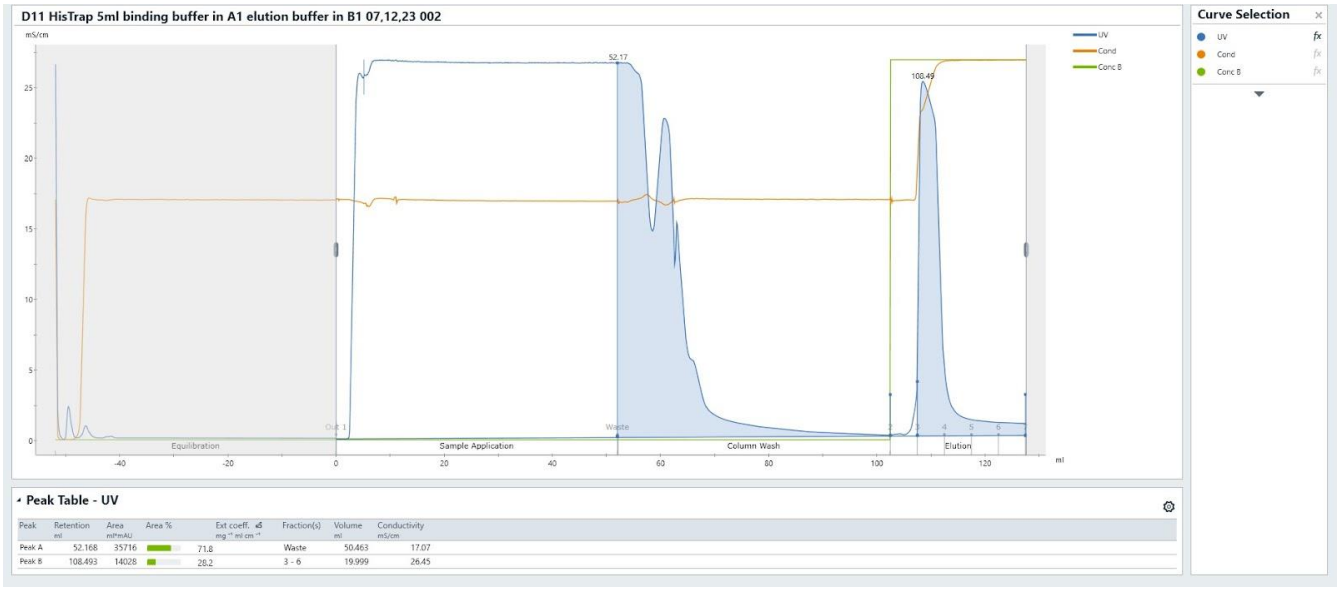

Fig. 11. Nickel affinity chromatogram of mutant D11.

Att. 11. Mutanta D11 niķeļa afinitātes hromatogramma.

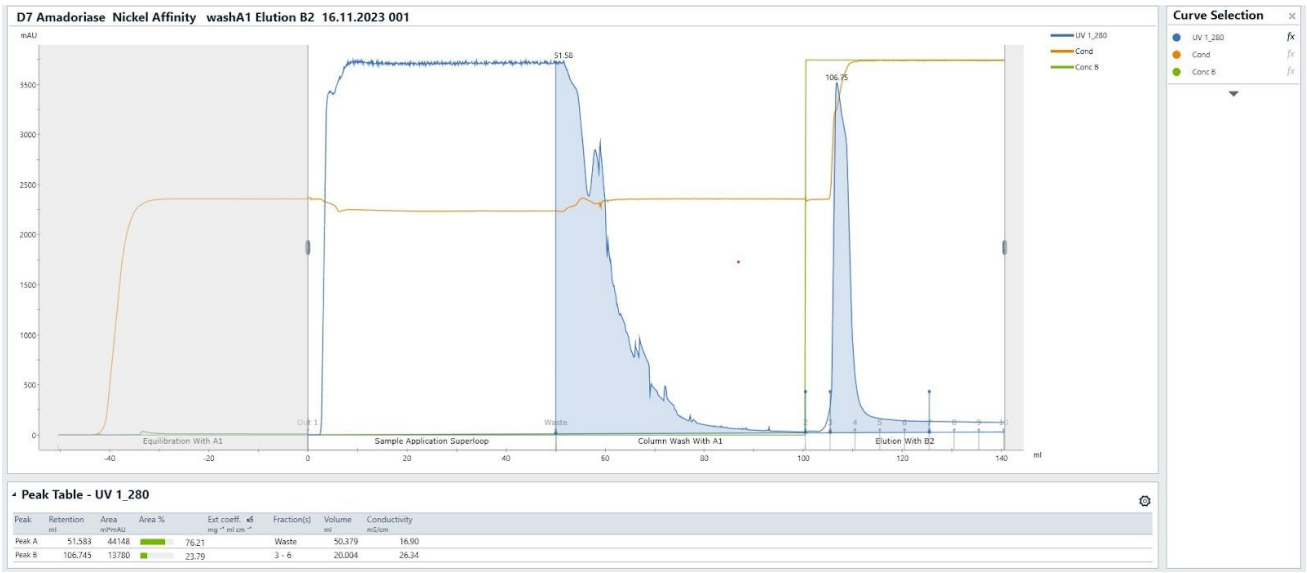

Fig. 12. Nickel affinity chromatogram of mutant D7.

Att. 12. Mutanta D7 niķeļa afinitātes hromatogramma.

Following Nickel affinity chromatography, we performed size exclusion chromatography to further purify the samples (Fig. 13 and Fig. 14). Samples were loaded into a pre equilibrated HiPrep 26/60 Sephacryl S-100 HR size exclusion column and passed through eluted from the column using SEC buffer. As sample passes through the size exclusion column, molecules with higher molecular weight elute faster than smaller ones, due to the porosity of the gel packed in the column. In chromatography, the presence of the protein of interest is assessed using absorbance at 280nm. After the two chromatography steps, we measured the concentrations of the best fractions using a NanoDrop. These fractions were then divided into 1-0.5 ml aliquots and flash frozen.

The final yield of D7 from 4 liters of bacterial culture was 72.5 mg, while the final yield of D11 was from 4 liters of culture was 99.5 mg.

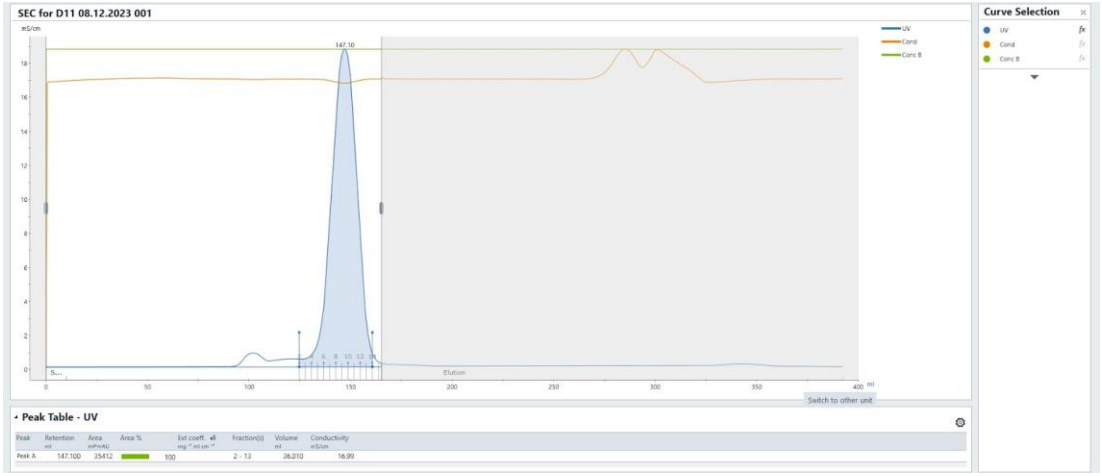

Fig. 13. SEC chromatogram of mutant D11.

Att. 13. Mutanta D11 *SEC* hromatogramma.

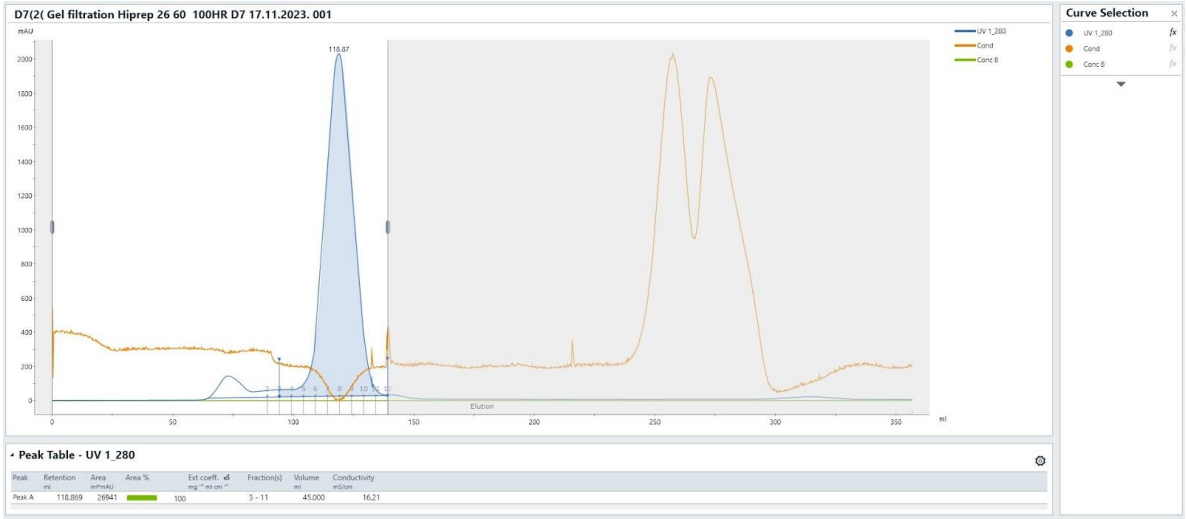

Fig. 14. SEC chromatogram of mutant D7.

Att. 14. Mutanta D7 *SEC* hromatogramma.

The results of the two purification steps for both proteins were assessed via gel electrophoresis. SDS-PAGE gels confirmed that both proteins were successfully produced and purified. In both cases, a visible band at 47kDa, the expected molecular weight of these mutants, could be observed.

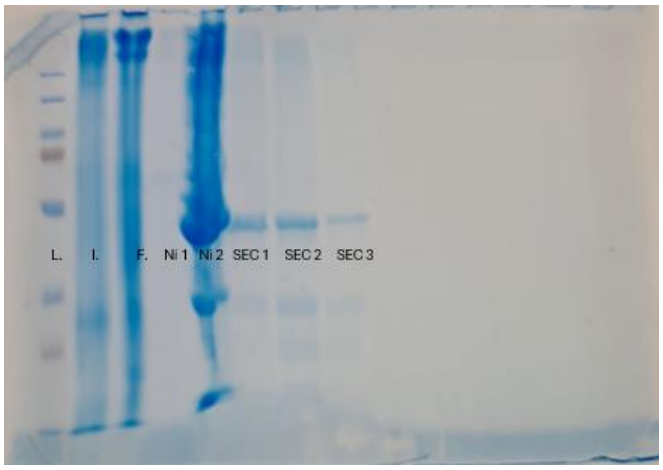

Fig. 15. SDS-PAGE of D7 showcasing various chromatography fractions

Columns: L. – Ladder; I.- Input; F- Flowthrough; Ni – nickel affinity fraction; SEC – size exclusion fraction

Att. 15. D7 *SDS-PAGE*, kurā redzamas dažādas hromatogrāfijas frakcijas

Kolonnas: L. – Marķieris; I. – Ievade; F – Caurplūde; Ni – niķeļa afinitātes frakcija; SEC – lieluma izslēgšanas frakcija

Fig. 16. SDS-PAGE of D11 showcasing various chromatography fractions.

Columns: L. – Ladder; I.- Input; F- Flowthrough; Ni – nickel affinity fraction; SEC – size exclusion fraction

Att. 16. D11 *SDS-PAGE*, kurā redzamas dažādas hromatogrāfijas frakcijas.

Kolonnas: L. –Marķieris; I. – Ievade; F – Caurplūde; Ni – niķeļa afinitātes frakcija; *SEC* – lieluma izslēgšanas frakcija

3.2 Melting curve analysis

We determined the melting temperature (Tm) and the secondary structures of the D7 and D11 mutants via circular dichroism. The analysis was done within a temperature range of 5°C to 90°C. The Tm of D7 was 56.67±0.07°C while the Tm of D11 was 58.00±0.11°C (Fig. 17 and Fig. 18, respectively). As previously mentioned, there can be a correlation between thrermostablility and yield as D11 is not only more thermostable but also has it has a better yield than D7. It is also important to mention that both enzymes are less thermostable than the mutant that they were based on – X02C. It had thermostability of 63.3±0.1°C, while also having a better yield, around 29 mg/L. These results also reinforce the idea that yield and thermostability are related.

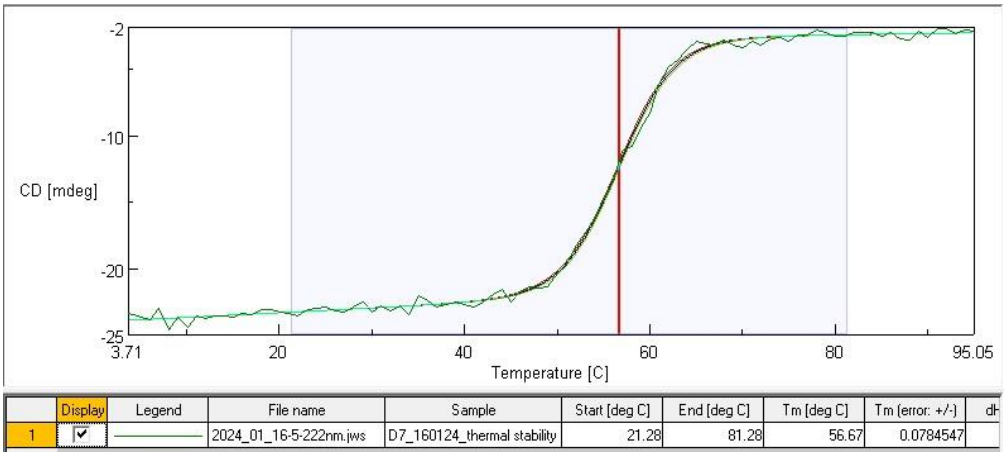

	Display	Legend	File name	Sample	Start [deg C]	End [deg C]	Tm [deg C]	Tm (error: +/-)	dH
1	☑		2024_01_16-5-222nm.jws	D7_160124_thermal stability	21.28	81.28	56.67	0.0784547	

Fig. 17. Melting curve analysis of the D7 mutant

Att. 17. D7 mutanta kušanas līknes analīze

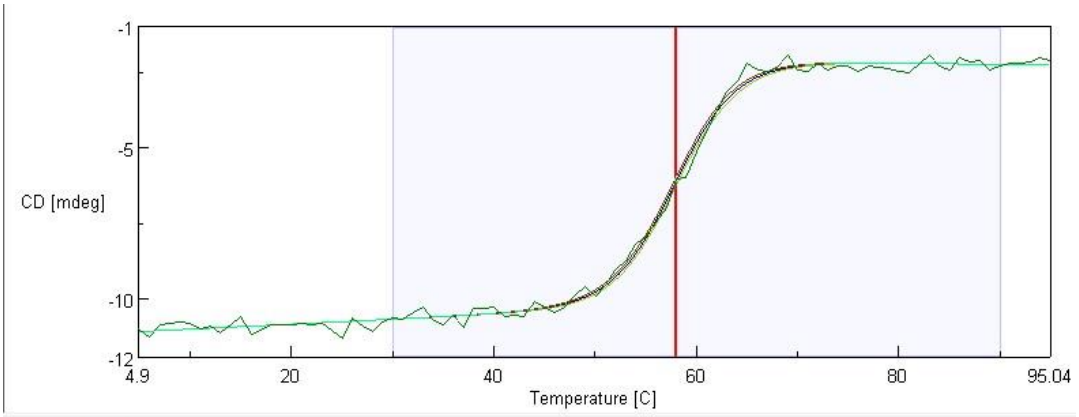

	Display	Legend	File name	Sample	Start [deg C]	End [deg C]	Tm [deg C]	Tm (error: +/-)	dH
1	☑		D11 tm.jws	D7 thermal stability	30.00	90.00	58.00	0.110723	

Fig. 18. Melting curve analysis of the D11 mutant.

Att. 18. D11 mutanta kušanas līknes analīze

3.3 Secondary structure analysis

To analyze the proteins using circular dichroism, I prepared the two protein samples at the concentration of 5mM. The analysis was done using a JASCO JA-1500 CD spectrometer and the secondary structure was analyzed using BeStSel software. Considering the observed curves, we concluded that both proteins were correctly folded (Fig. 19 and Fig. 20). Secondary structure content of D11 showed that 76.3% of the structure were alpha helixes, with 69.9% regular helixes and 6.4% distorted helixes. The structure of D7 had a 87.5% content of alpha helixes, with 80.6% of regular helixes and 6.8% of distorted helixes. This indicated slight structural differences between the mutants.

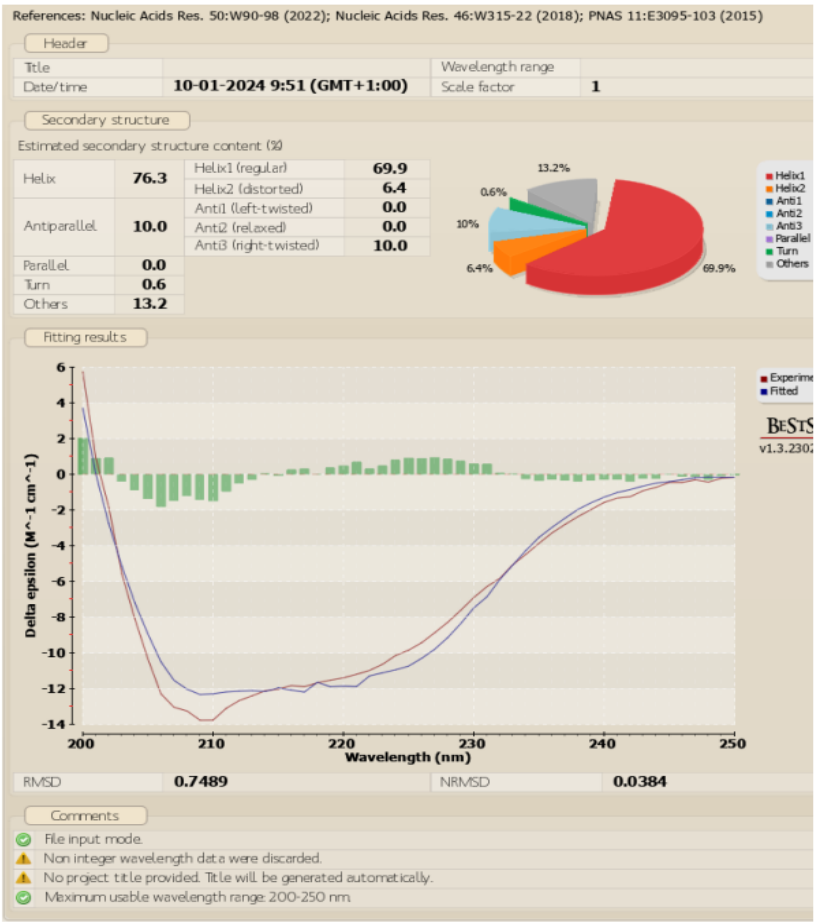

Fig. 19. Secondary structure analysis of D11 calculated using BeStSel software

Att. 19. D11 sekundārās struktūras analīze, kas ir aprēķināta, izmantojot BeStSel programmatūru

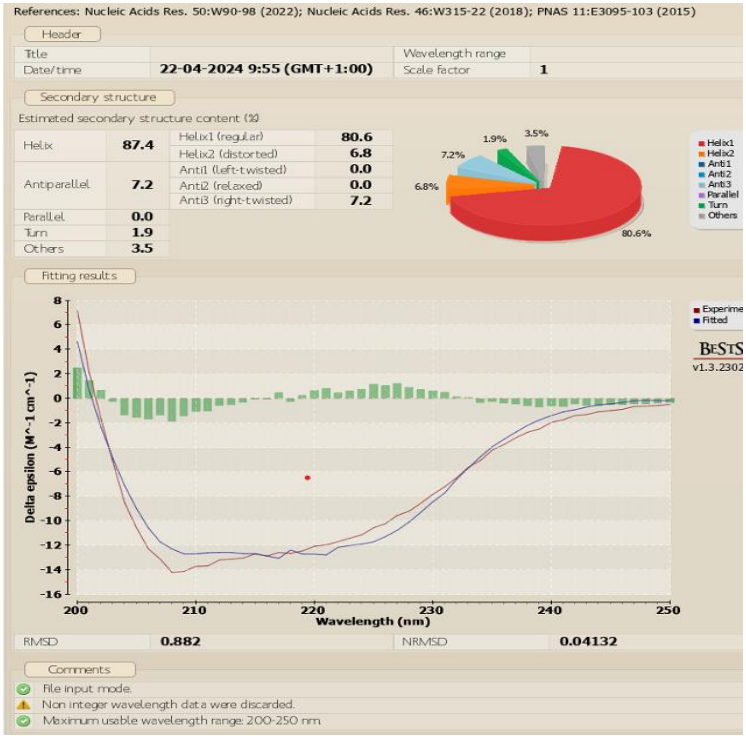

Fig. 20. Secondary structure analysis of D7 calculated using BeStSel software

Att. 20. D7 sekundārās struktūras analīze, kas ir aprēķināta, izmantojot BeStSel programmatūru

3.4 Enzymatic assay analysis

To assess the activity of the two mutants, we performed enzymatic assays on the natural substrate (fructosyl-valine) and on the fructosyl hexapeptide derived from the 6 N-terminal residues of HbA1c, which represents a larger substrate than the natural one. In this assy, we measured the production of glucosone over time by monitoring absorption at 322nm.

In order evaluate the activity of the mutants it is necessary to calculate the absorption change rate by dividing the difference of the absorption by the time of the reaction. Using this value, it becomes possible to calculate substrate conversion rate using previously acquired data and dividing it by the extinction coefficient of the glucosone and path length. The catalytic activity of the enzyme is calculated by dividing conversion rate of the substrate by the volume of the reaction. The specific activity of the enzyme is calculated by dividing the enzyme activity by enzyme concentration expressed in mg/ml.

With respect to the natural substrate (fructosyl-valine), D7 had specific enzymatic activity of 26,22 ± 1,084 $\mu mol * min^{-1} * mg^{-1}$ while D11 had 26,212 ± 1,273 $\mu mol * min^{-1} * mg^{-1}$.

Both of these enzymes showed improved specific activity compared to their parent enzyme, X02C, which was reported to have specific activity of only 17.95 ± 2.46 μmol∗min^{-1}∗mg^{-1}. These finding suggest that mutations that were introduced near the active site, not only did not interfere with the activity of the towards shorter substrates, but improved it. Looking at this data we can conclude that the mutations restored the ability of their parent enzyme (X02C) to process fructosyl-valine almost to the same level as the wild type enzyme (29.67 ± 2.56 μmol∗min^{-1}∗mg^{-1}).

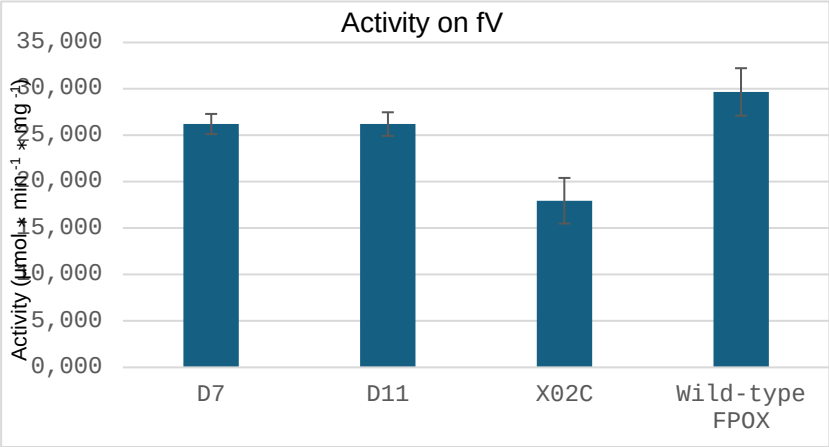

Fig. 21. Specific activity of the tested mutants on the fructosyl-valine substrate

Att. 21. Pārbaudīto mutantu specifiskā aktivitāte uz fruktosilvalīna substrātu

On the other hand, the enzymatic assays showed that, when tested on the fructosyl hexapeptide, both enzymes had worse activity compared to their parent enzyme. This may suggest that the changes in the active site only benefited small substrate recognition, while inhibiting recognition of the larger one. Comparing the observed data to previously published data, we could see that the activity was almost two times worse. Specific activity of X02C was $0{,}43 \pm 0{,}06$ μmol∗min^{-1}∗mg^{-1} (Estiri et al. 2023), while the specific activity of D7 and D11 on fructosyl hexapeptide is $0{,}216 \pm 0{,}006$ μmol∗min^{-1}∗mg^{-1} and $0{,}217 \pm 0{,}010$ μmol∗min^{-1}∗mg^{-1}, respectively. We can see that D11 had better activity, but considering standard deviation, difference is negligeable. It is also important to mention that all the mutants possess worse activity than wild type enzyme, $0{,}78 \pm 0{,}09$ μmol∗min^{-1}∗mg^{-1}.

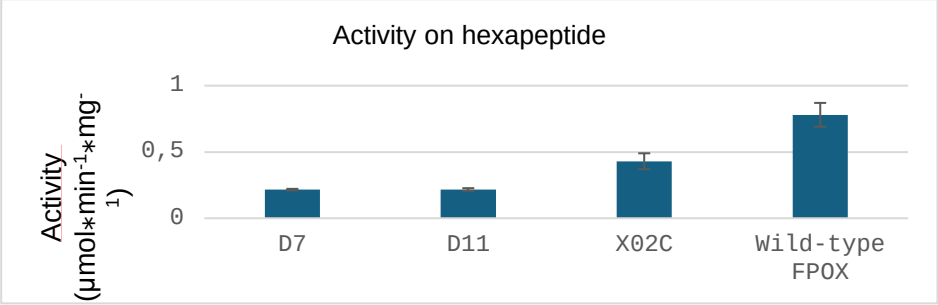

Fig. 22. Specific activity of the tested mutants on the fructosyl-hexapeptide substrate

Att. 22. Pārbaudīto mutantu specifiskā aktivitāte uz fruktosilheksapeptīda substrātu

3.5 Protein crystallization

In order to analyze if the goal of enlarging the active site has been achieved, we needed to produce the crystal structure of the two mutants. To this end, we use the hanging drop vapor diffusion method to produce suitable crystals for x-ray diffraction data collection.

In crystallization experiments, different concentrations of the precipitant and of the protein can lead to a different placement on the solubility curve (Fig. 23). If the concentrations are too low, they enter metastable zone. In the metastable zone the concentration is too low for crystals to form or for sample to undergo nucleation. If the concentrations are too high, they enter the precipitation zone. Precipitation zone is unfavorable as it leads to aggregation of the sample. Protein forms amorphous precipitate, as such formation of crystals is impossible. The best odds for crystal formation is in the liable zone, as it has the best odds of nucleation.

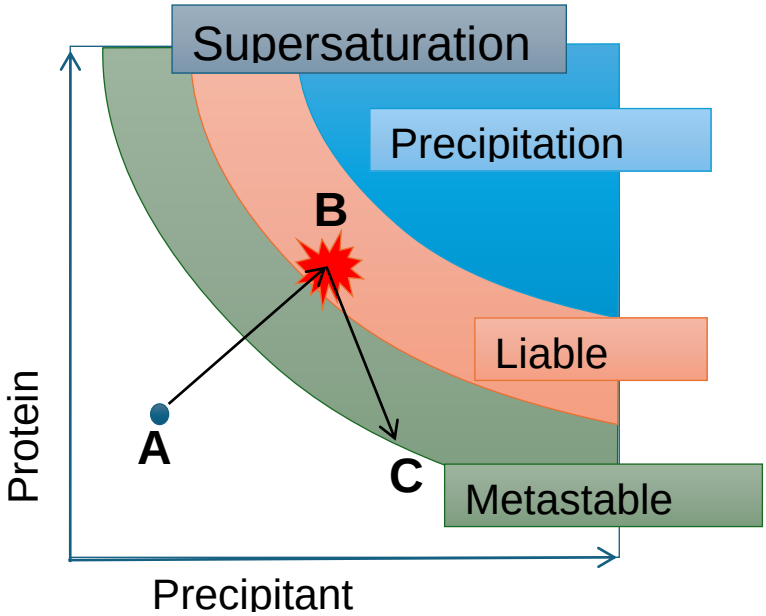

Fig. 23. Solubility diagram in crystallization experiments

Att. 23. Šķīdības diagramma kristalizācijas eksperimentos

Our first crystallization attempts utilized the same conditions as the ones that were used to crystallize the previous generation of mutants. In 24 well hanging drop plate we have added crystallization condition containing 0.1M of MES and concentration of PEG ranging from 36% to 16% of various molecular weight (20kDa, 8kDa, 6kDa, 4kDa). For our experiments we used protein at the concentration of 10 mg/ml. After setting up a plate and leaving it in a crystallization room at a constant temperature of 20˚C for two days it became obvious that this condition was not going to afford crystals as in all of the drops there was visible precipitation.

Our further attempts were mostly focused on changing the pH of our crystallization buffers based on the isoelectric point of the two mutants. It is well known that for successful crystallization experiments, it is important to avoid being too close to the isoelectric point of the protein being tested. The isoelectric point of mutant D7 is 6.9., so we tested tow buffers, one at a higher pH (0.1 M Tris pH 8.0) and one at a lower pH (0.1 M Sodium citrate pH 5.6). After setting up the plates there was a clear difference between these two conditions. The condition with 0.1 M sodium citrate pH 5.6 featured also different molecular weight PEGs at different concentrations, ranging from 18% to 8%. The plate showed heavy precipitation, especially in the wells with higher PEG concentration and with high molecular weight PEG. All signs pointed that the acidity of the buffer had a detrimental effect on the crystallization. Indeed, the plate with 0.1 M Tris 8.0 had much better results. We could observe crystal formations in the wells where PEG was present at high concentration. Best results were observed various crystals formation in wells containing PEG 8K and PEG 20K. Crystals were easy to spot and usually formed crosses and overall morphology was rather poor as they appeared to be very thin (Fig. 24). This is never desirable as it can lead to anisotropy during diffraction data collection, which results in poor resolution and poorly defined parts of the electron density map.

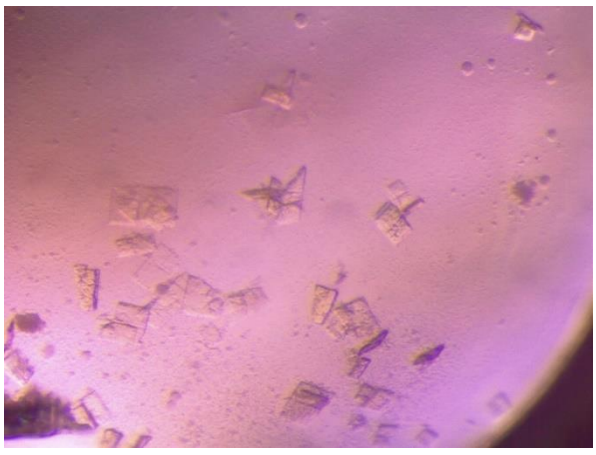

Fig. 24. Crystals of D7 formed in 0.1 M Tris pH 8.0 and 12% PEG 8K

Att. 24. D7 kristāli, kas veidoti 0.1 M Tris pH 8.0 un 12% PEG 8K

After obtaining these crystals we focused on improving their morphology. At first, we attempted crystallization in the same conditions but placing the plate at 4°C. To observe the appearence of the first crystals, we had to wait a longer time due to the lower temperature of the experiment and the slower evaporation of the drop. The previous plate was kept at 20°C and it was possible to observe crystals on the next day, while at 4°C plate we could observe crystals only after one week. Nevertheless, the results were quite similar and crystals still had the same morphology issues (Fig. 25). It was possible to observe tiny rectangular crystals in many of the wells. It is also important to mention that we could observe an increase in crystal count, but decrease in their size. New crystals from this plate were still not suitable for data collection, as they were too small. Nevertheless, this data gave us a good reference point for further rounds of optimization.

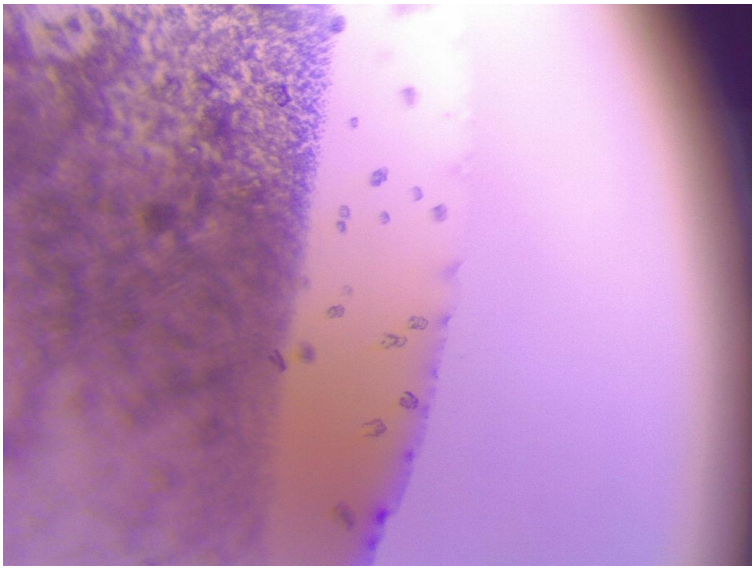

Fig. 25. Crystals of D7 obtained in 0.1M Tris pH 8.0 and 16% PEG 8K, at 4°C

Att. 25. D7 kristāli, kas iegūti 0.1M Tris pH 8.0 un 16% PEG 8K, pie 4°C

Our next crystallization condition included 5% concentration of ethanol, which is an addictive known to improve the size of small crystals when a large number of tiny crystals are obtained. After waiting for a week, we observed an improved crystal growth. Crystals were bright yellow, which meant that they were protein crystals. Additionally, they were much bigger than in the previous plate and had a better morphology (Fig. 26). These were the crystals that we used to collect diffraction data.

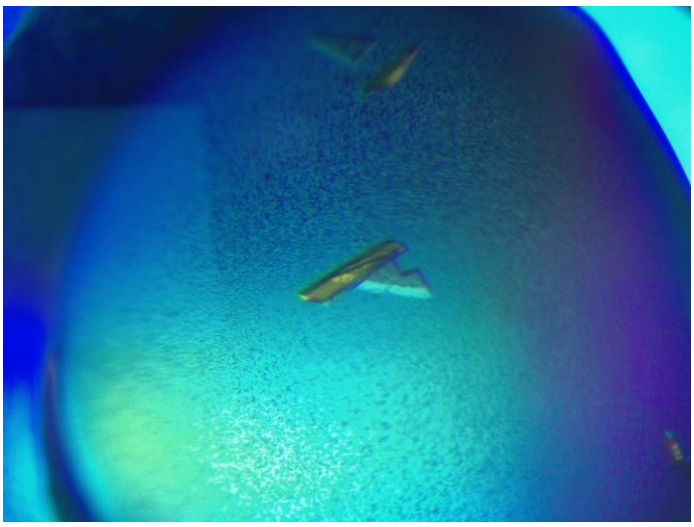

Fig. 26. Crystals of D7 formed in 0.1M Tris pH 8.0, 5% ethanol, 12% PEG 8K, at 4°C

Att. 26. D7 kristāli, kas veidoti 0.1M Tris pH 8.0, 5% etanolā, 12% PEG 8K, pie 4°C

Our attempts at crystallization of D11 mutant were similar. After achieving crystals of D7 in a condition with pH one point higher than mutant's isoelectric point, we attempted the same approach with the D11 mutant. The isoelectric point of D11 is 7.6. Hence, conditions included 0.1M Tris pH 8.6 and various PEG concentrations, ranging from 18% to 8%. Nevertheless, the plate did not produce any crystals (Fig. 27).

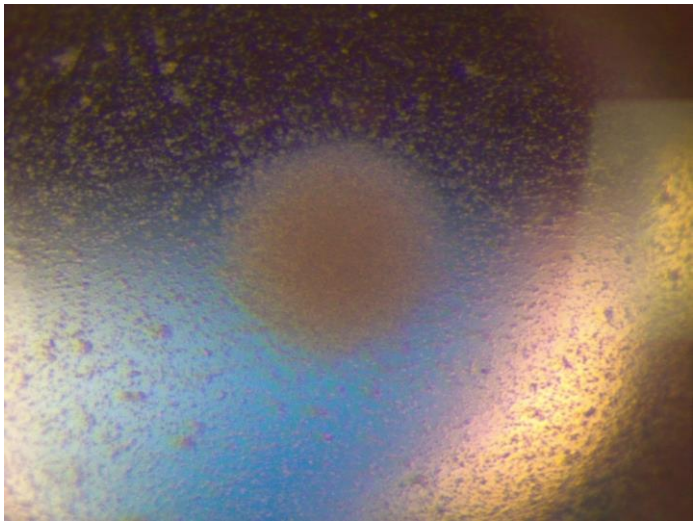

Fig. 27. Precipitation of D11 in conditions containing 0.1 M Tris pH 8.6 and 16 % PEG 8K.

Att. 27. D11 izgulsnēšanās apstākļi, kas satur 0.1 M Tris pH 8.6 un 16 % PEG 8K.

Our next attempts were focused on changing various aspects of this condition. We attempted raising the pH to 8.8 and 9.0. Both of these plates showed varying levels of precipitation. Lowering the pH of Tris to 6.6 also did not produce any notable results. All the wells displayed varying levels of precipitation with no sign of nucleation. Furthermore, we tried changing the chemical nature of the buffer. We have made a plate where we used 0.1 M Hepes pH 8.6 and the same concentrations of PEG. However, the plate displayed much worse results compared to a plate with Tris at the same pH. Another plate with CHES buffer at the same pH also did not show any sign of nucleation. Considering how ethanol presence and temperature change positively impacted D7 crystallization, we attempted a similar approach for D11 mutant. A plate was set up with Tris at pH of 8.6, and 5% ethanol and left at a temperature of 4°C for a week. Unlike D7 this plate showed only light precipitation and no crystal formation. Furthermore, increasing the concentration of the protein in the drop also did not seem to yield any results.

3.6 Crystal structure solution

After achieving crystallization of the D7 mutant, it was important to cryopreserve protein crystals for later storage and analysis. We used a mixture of 25% glycerol as cryoprotectant. Crystals were harvested with an appropriately sized cryo-loop mounted on a magnetic pin. After all the crystals were harvested and placed in a dewar chilled with liquid nitrogen they are sent to Diamond Light Source synchrotron for X-ray diffraction analysis. After getting X-ray diffraction data, we used Molecular Replacement and the previously determined crystal structure of mutant X02B as a search probe to solve the structure of the D7 mutant.

The first data set that we collected with the initial crystals of D7 had a resolution of 2.5 Å and an overall completion of 96.6%. The relatively low resolution of this data set was expected as crystals were thin and featured a poor morphology. Nevertheless, the data set showed no evidence of twinning or ice rings. After initial molecular replacement, we obtained R and R_{free} values of 0.26 and 0.29.

After performing molecular replacement, we had to mutate various residues in region of amino acid number 60 to 70, as this region was changed in X02B. This was done by manually mutating the residues into the appropriate ones and fitting them in the electron density map using the software Coot. After preforming a refinement using Refmac5, we concluded that the mutations were indeed present as the changes fit the electron density map.

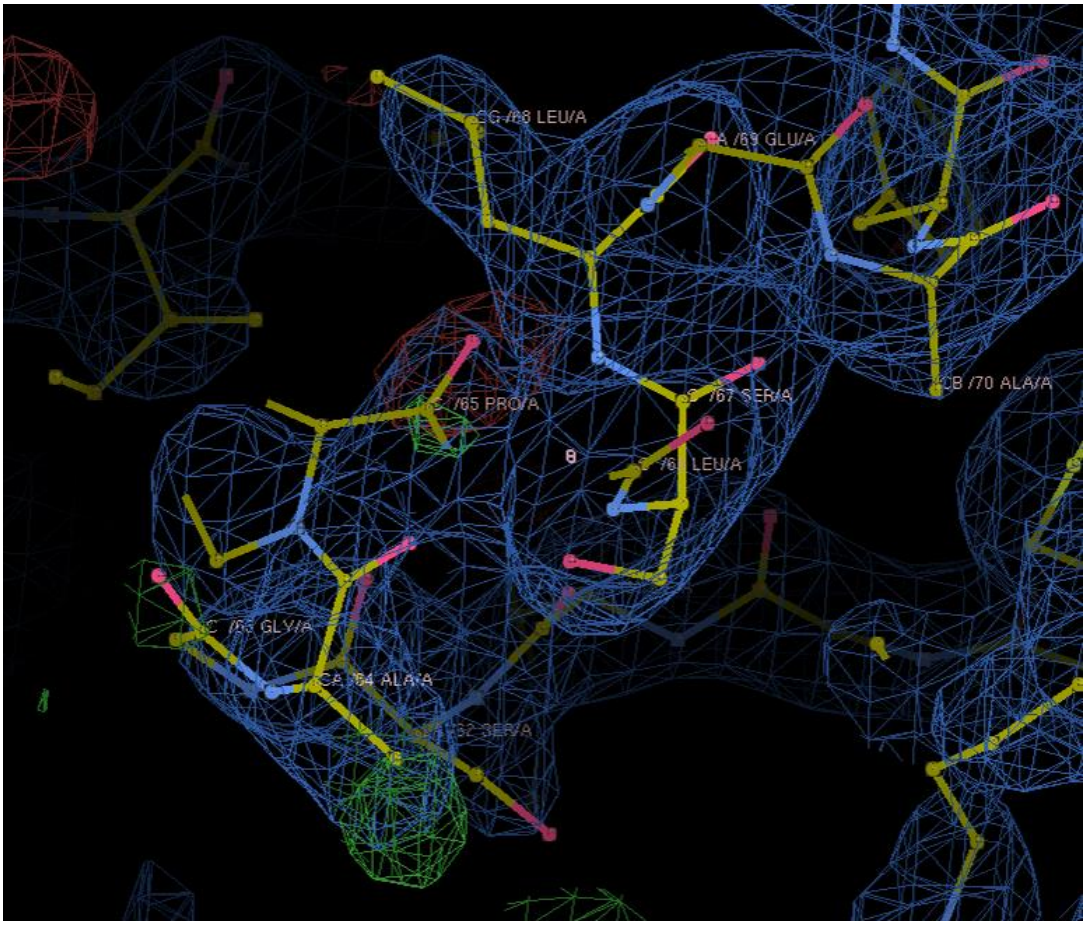

Fig. 28. Model fitting in the 60th to 70th residue's region.

Att. 28. Modeļa pielāgošana no 60.līdz 70. aminoskābei.

Our attention was later set on placing FAD, enzyme's cofactor, correctly. As the polymer model that we used as a basis did not include water atoms and, more importantly, ligand, we had to place it manually. It was done manually by importing the .CIF library of the ligand. This library allows the program to make appropriate calculations in order to fit the molecule in relation to the polymer. After the import of the library we could place a structure of the FAD in the appropriate region of the electron density map. Just like in the previous crystal structures, FAD is placed near the active site. It was necessary to adjust the molecule so that it would correctly fit into the electron density map. When it was done and the structure was refined it improved R_{free} value from almost 0.3 to 0.28, which meant that the inclusion of the FAD was beneficial to the overall structure.

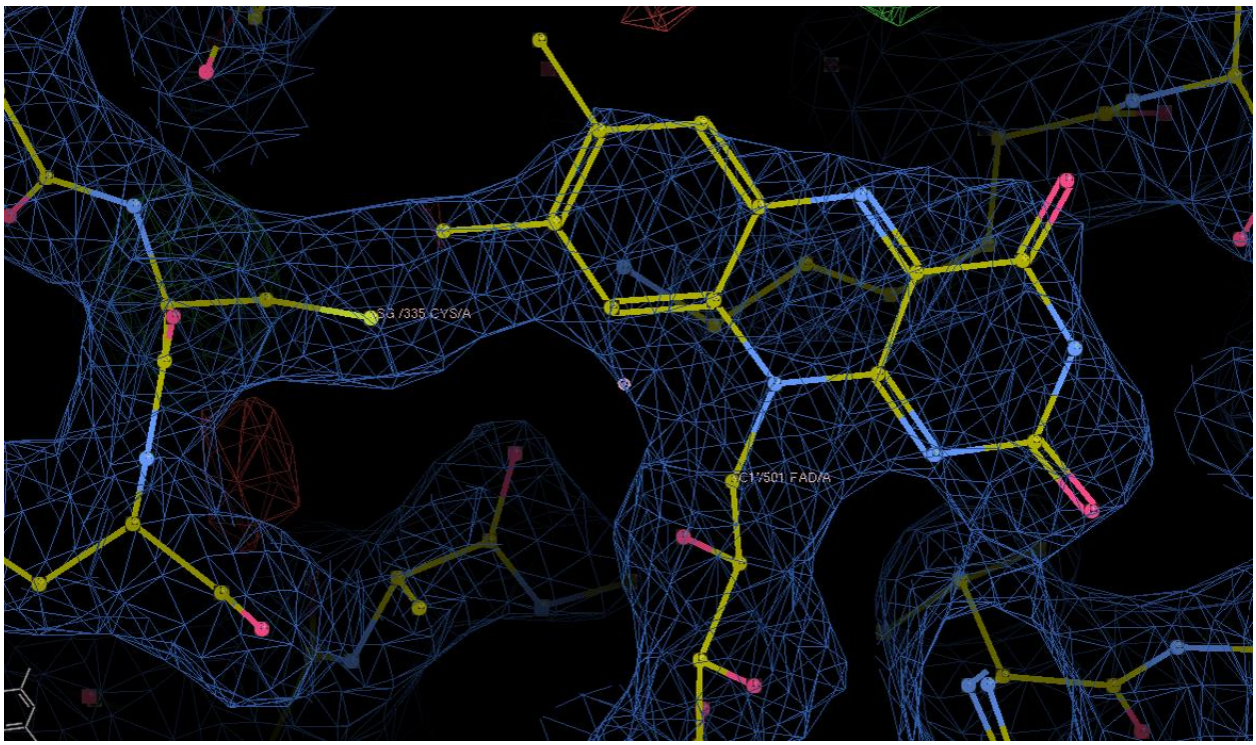

Fig. 29. Model fitting of FAD.

Att. 29. FAD modeļa pielāgošana.

After appropriately fitting FAD, our attention was put on the engineered portion of the protein. Firstly, we needed to manually remove all the changed residues, as it is much easier to reconstruct the changed position manually. After removing all the residues in their places alanine was inserted as it is the simplest amino acid. After adding the appropriate amount of alanines, they are later changed into an appropriate amino acid using the mutate function and placed correctly within the electron density map. Electron density map showed that indeed the alpha helix was 3 amino acids shorter in the appropriate region, thus we can conclude that the mutations were successful and our goal of changing the structure was met.

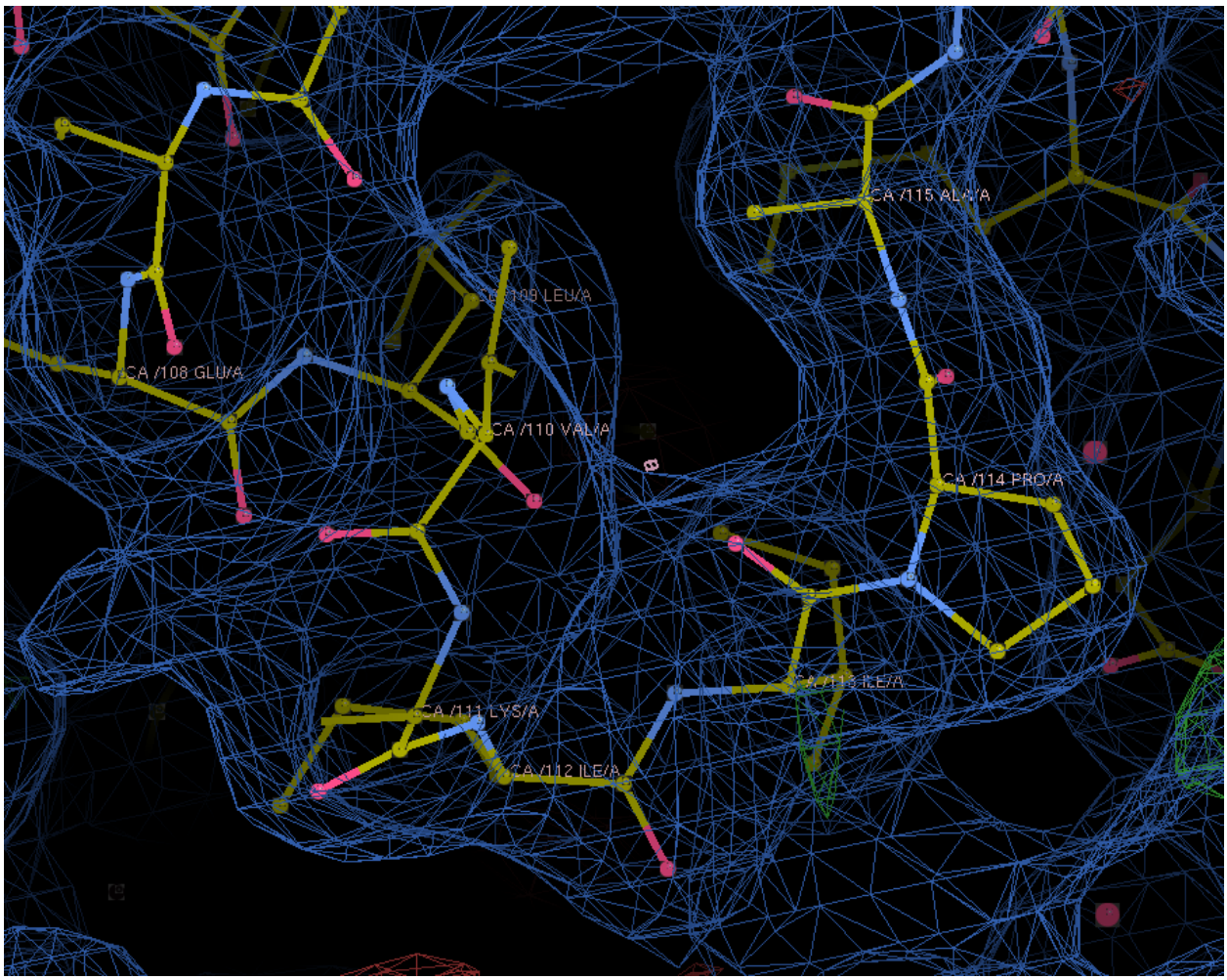

Fig. 30. Model fitting in the engineered site.

Att. 30. Modeļa pielāgošana inženērētajā vietā

Nevertheless, model possessed multiple problems and poor crystal quality impacted the quality of the electron density map. While resolution was acceptable and the model complete, which meant that we could assess how the mutant was changed, the structure did not appear of good quality. For instance, in the region from the 300th to the 420th residue, several parts of the electron density map were missing. This means that we could not confidently place amino acids in the electron density map.

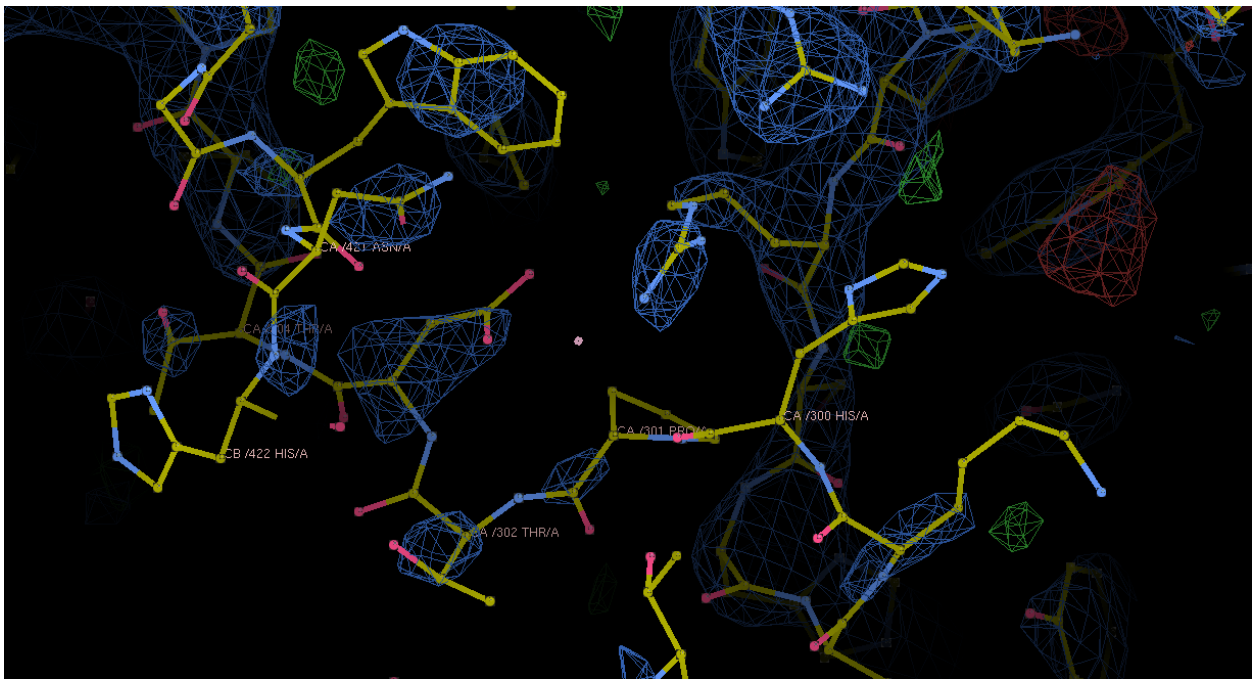

Fig. 31. Model fitting using poor quality diffraction data

Att. 31. Modeļu pielāgošana, izmantojot nekvalitatīvus difrakcijas datus

At this stage, our focus turned onto collecting a better diffraction data set. Crystals grown in 0.1M Tris pH 8.0, 5% ethanol and kept at 4°C seemed to possess a better morphology, hence to be promising candidates for obtaining a better and higher resolution X-ray diffraction data set (Fig. 26).

We collected x-ray diffraction data again at the DIAMOND light source in Oxford. With this new data seti, the structure was solved by molecular replacement following the same protocol described for the previous above and refined at 2.1 Å resolution. This led to the calculation of a good quality electron density map which allowed us to full refine the structure without any major problem. The structure was refined to a final R factor of 19.9 and R_{free} of 25.5, which are both indicative of a much better quality of data compared to the structure that we obtained from the initial crystals (see crystallographic table). In the following, some portions of the electron density map are shown to provide evidence of the quality of the new structural determination. These include close up figures of the disulphide bond introduced for thermal stabilization (Fig. 32), the FAD cofactor (Fig. 33) and the region where the mutations have been introduced in this particular mutant (Fig. 34).

Crystallographic table

	FPOX_D7
Wavelength (Å)	0.97627
Resolution range (Å)	53.92 - 2.093 (2.168 - 2.093)
Space group	P1
Unit cell (Å, º)	54.083 54.12 82.657 80.071 85.533 89.837
Total reflections	170539 (7773)
Unique reflections	52616 (5242)
Multiplicity	3.2 (3.0)
Completeness (%)	96.89 (95.66)
Mean I/sigma(I)	5.2 (1.1)
Wilson B-factor	35.86
R-merge	0.126 (1.221)
R-meas	0.149 (1.479)
R-pim	0.079 (0.822)
CC1/2	0.982 (0.357)
Reflections used in refinement	52603 (5241)
Reflections used for R-free	2614 (275)
R-work	0.1994 (0.3034)
R-free	0.2552 (0.3453)
Number of non-hydrogen atoms	6995
macromolecules	6605
ligands	118
solvent	272
Protein residues	832
RMS(bonds)	0.012
RMS(angles)	2.13
Ramachandran favoured (%)	96.01

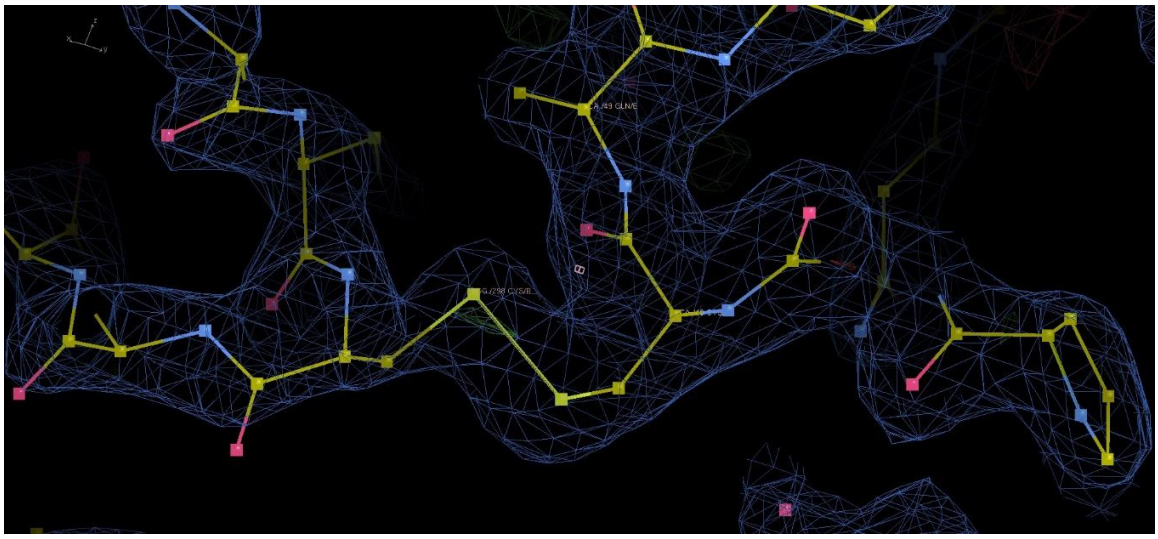

Fig. 32. Disulphide bond between Cys 48 and Cys 296. This disulphide bod was introduced in one of the previous rounds of engineering.

Att. 32. Disulfīdu tiltiņs starp Cys 48 un Cys 296. Šis disulfīda tiltiņš tika ieviests vienā no iepriekšējām inženērijas kārtām.

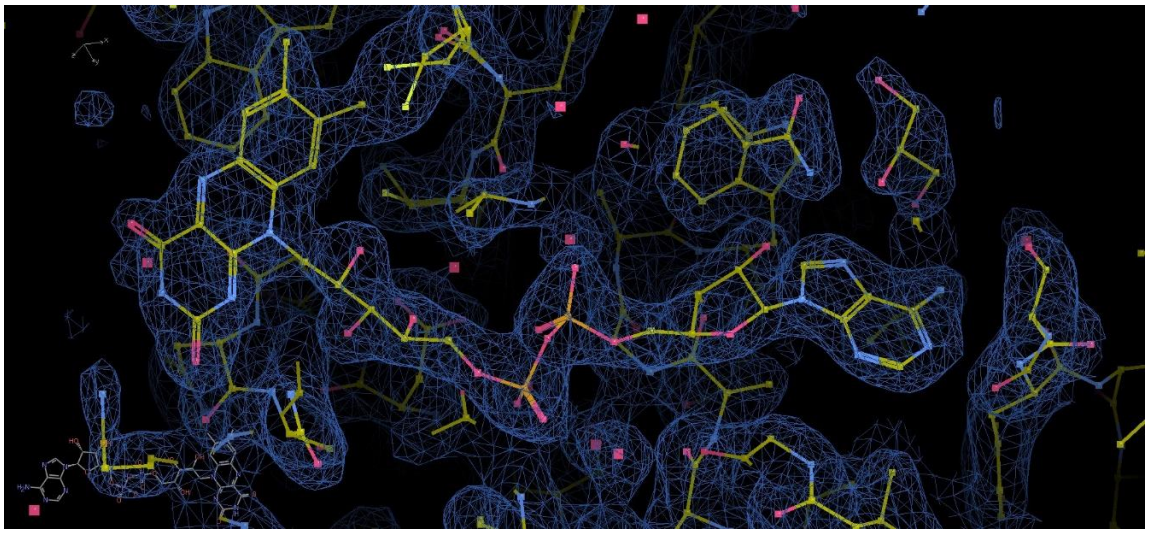

Fig. 33. The FAD cofactor was clearly visible in the electron density map.

Att. 33. FAD kofaktors bija skaidri redzams elektronu blīvuma kartē.

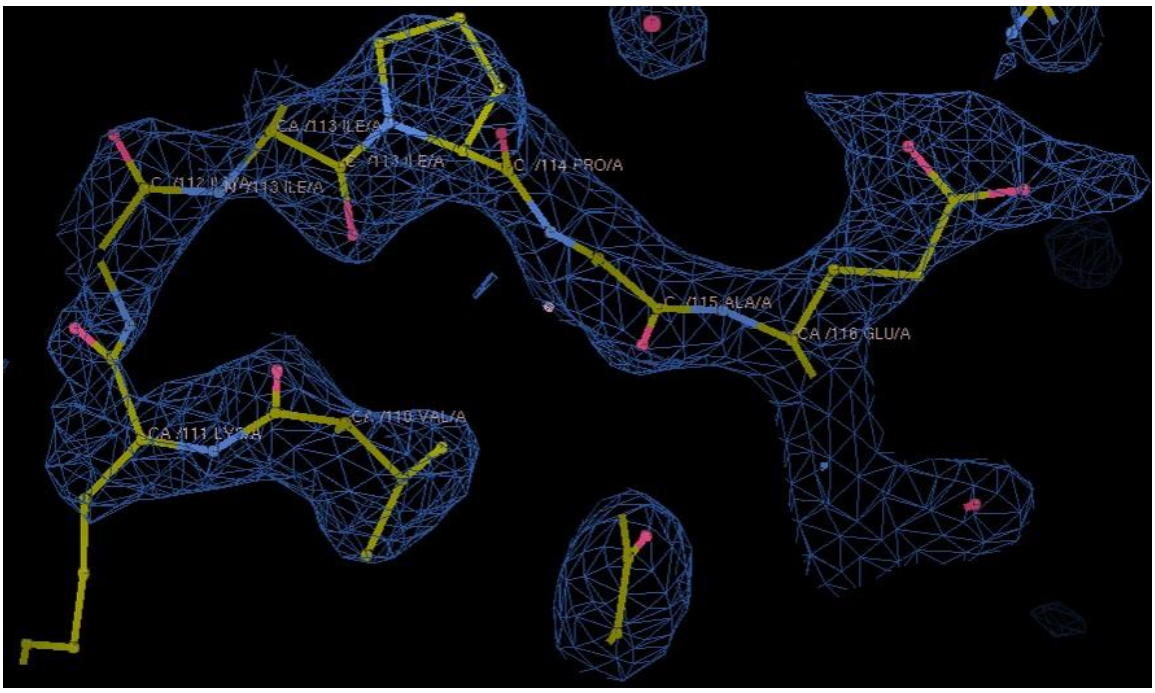

Fig. 34. Clear electron density could be seen in the mutated area of the enzyme.

Att. 34. Skaidri redzāms elektronu blīvums enzīmu mutācijas zonā.

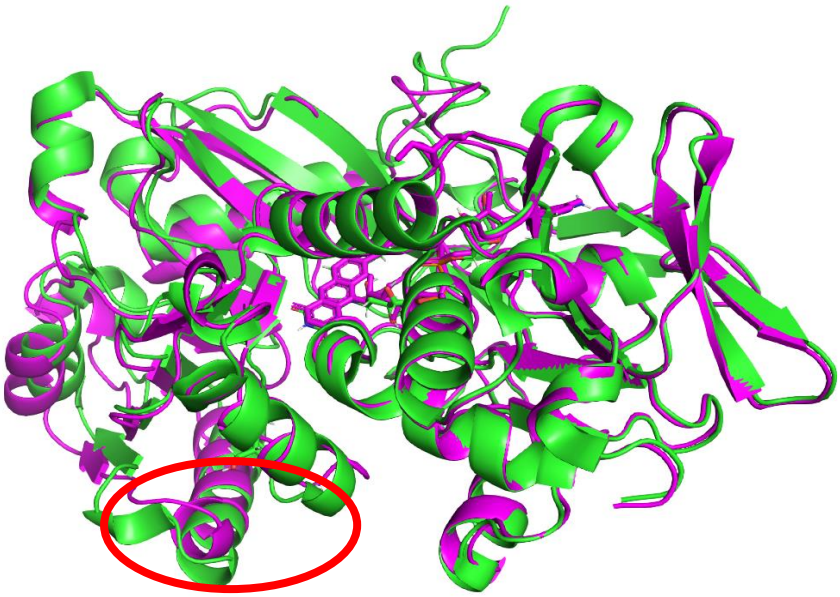

Fig. 35. Superposition of the crystal structure of D7 and the crystal structure of X02B, which was used as a probe for molecular replacement (rmsd: 1.5 Å)

Att. 35. D7 kristāla struktūras un X02B kristāla struktūras superpozīcija, ko izmantoja kā paraugu molekulārai nomaiņai (rmsd: 1.5 Å)

Currently, we are in the process of solving and refining additional crystal structures from this round of engineering. When some of the currently missing structures are obtained, it will be possible to compare all the new mutants and derive clear indications of the effect of the mutations on the enzyme. Considering that none of the new mutants is active on large substrates such a fructosyl-hexapeptide, it is unlikely that this set of mutations will have a noticeable effect on widening of the tunnel that leads to the catalytic pocket of the enzyme. Further mutations will have to be considered.

Regarding the two mutants described herein, overall, both mutants show good expression levels, both of them producing more than 50 mg from 4 liter cultures. Additionally, they both show better thermostability, compared to the wild type FPOX with D11 needing 5°C higher melting temperature. Nevertheless, both mutants show worse performance compared to the parent enzyme, X02C which had more than 60 mg yield and melting temperature of almost 64°C. However, both mutants show increased activity towards small substrate, fructosyl-valine when compared to X02C, with nearly 10 $\mu mol * min^{-1} * mg^{-1}$ increase. This means that the mutants had their ability to bind to smaller substrates restored on the level of the wild-type FPOX, while gaining increased yield and thermostability from their parent enzyme. It is also important to mention that the mutations introduced near active site may have inhibited their ability to bind to larger substrates with D7 and D11 having specific two times less compared to X02C. Data obtained from D7 X-ray diffraction crystallography showcases that mutation did impact the crystal structure of the FPOX and electron density map corresponds to the theoretical placements of the amino acids. Currently, we are trying to obtain the crystal structures of the other mutants that we designed in the round if engineering. Altogether, these mutants will be used as a basis for further rounds of rational design modeling in order to further improve substrate recognition. X-ray crystallography data obtained from this study can be used as data to improve the algorithms used for enzyme engineering, thus making the process faster and more efficient.

CONCLUSIONS

1. Both FPOX mutants, D7 and D11, were successfully expressed and purified
2. D11 had better yield and thermostability compared to D7
3. Both mutants showed worse expression and thermostability compared to their parent enzyme, X02C
4. Both mutants showed better activity on fructosyl-valine compared to their parent enzyme X02C
5. D7 and D11 did not show enhanced activity on fructosyl-hexapeptide
6. It was possible to crystallize D7 and to solve its crystal structure at 2.1 Å resolution.

ACKNOWLEDGEMENTS

I would like to express my gratitude to the whole Biotechnology group of LIOS, especially to Dr. Emilio Parisini, head of the group and my thesis advisor, for introducing me to the laboratory's techniques, with patience and support. Special thanks also to Shapla Bhattacharya for looking over my shoulder and providing constant help throughout the entire thesis.

BIBLIOGRAPHY

1. Andreas J. H., Michael W., Thierry H., (2011) Chapter ten - Glycoprotein Maturation and the UPR, Methods in Enzymology, Academic Press, 491, 163-182

2. Chaudhuri J., Bains Y., Guha S., Kahn A., Hall D., Bose N.,Gugliucci A., Kapahi P. (2018). The role of advanced glycation end products in aging and metabolic diseases: bridging association and causality. Cell metabolism, 28(3), 337-352.

3. Estiri H., Bhattacharya S., Buitrago J. A. R., Castagna R., Legzdiņa L., Casucci G., Ricci A., Parisini E., Gautieri A., (2023) Tailoring FPOX enzymes for enhanced stability and expanded substrate recognition, Sci Rep, 13, 18610

4. Haque S., Siddiqui R., (2013) Clinical Significance of Glycated Hemoglobin (HbA1c) AKMMC J: 4(1)

5. Internation Diabetes Association (2024) Facts and Figures https://idf.org/about-diabetes/diabetes-facts-figures/

6. Kaushansky K., Lichtman M., Prchal J., Levi M., Burns L., Linch D., (2021) Williams Hematology, 10th Edition

7. Lan Z., Pingping W., Jixin Z., Chao X., Jingguo X., Huiqing X., Guiyou C., Jun W., (2023) Effects of exogenous advanced glycation end products on oxidative stress and renal injury in healthy mice. eFood, 4(4), e105

8. Mastrocola R., Collotta D., Gaudioso G., Le Berre M., Cento A. S., Ferreira A. G., Chiazza F., Verta R., Bertocchi I., Manig F., Hellwig M., Fava F., Cifani C., Aragno M., Henle T., Joshi L., Tuohy K., Collino M., (2020) Effects of Exogenous Dietary Advanced Glycation End Products on the Cross-Talk Mechanisms Linking Microbiota to Metabolic Inflammation. Nutrients. 19;12(9):2497.

9. Martins S., Jongen W., Boekel M., (2002) A review of Maillard reaction in food and implications to kinetic modelling, Trends in Food Science & Technology, 11(9-10), 364-373

10. Nedić O., Rattan S. I. S., Grune T., & Trougakos, I. P., (2013) Molecular effects of advanced glycation end products on cell signalling pathways, ageing and pathophysiology. Free Radical Research, 47(sup1), 28–38.

11. Nessar A., (2005) Advanced glycation endproducts—role in pathology of diabetic complications, Diabetes Research and Clinical Practice, 67 (1), 3-21,

12. Nowotny K., Schröter D., Schreiner M., Grune T., (2018) Dietary advanced glycation end products and their relevance for human health, Ageing Research Reviews, 47, 55-66

13. Prasad C., Davis K.E., Imrhan V., Juma S., Vijayagopal P., (2017) Advanced Glycation End Products and Risks for Chronic Diseases: Intervening Through Lifestyle Modification. Am J Lifestyle Med. 15;13(4):384-404.

14. Qinghe S., Junjun L., Liyuan D., Xiaolei W., Xiandang Z., (2021) Novel advances in inhibiting advanced glycation end product formation using natural compounds, Biomedicine & Pharmacotherapy, 140,111750.

15. Rigoldi F., Donini S., Giacomina F., Sorana F., Redaelli A., Bandiera T., Parisini E., Gautieri A., (2018) Thermal stabilization of the deglycating enzyme Amadoriase I by rational design. Sci Rep 8, 3042

16. Rigoldi F., Donini S., Torretta A., Carbone A., Redaelli A., Bandiera T., Parisini E., Gautieri A., (2020) Rational backbone redesign of a fructosyl peptide oxidase to widen its active site access tunnel, Biotechnology and bioengineering, 117(12), 3688-3698.

17. Rigoldi F., Gautieri A., Vedove A., Lucarelli A., Vesentini S., Parisini E., (2016), Crystal structure of the deglycating enzyme Amadoriase I in its free form and substrate-bound complex. Proteins. 84(16), 744-758.

18. Rondeau P., Bourdon E., (2011) The glycation of albumin: Structural and functional impacts, Biochimie, 93(4), 645-658,

19. Rungratanawanich W., Qu Y., Wang X., (2021) Advanced glycation end products (AGEs) and other adducts in aging-related diseases and alcohol-mediated tissue injury. Exp Mol Med 53, 168–188

20. Salazar J., Navarro C., Ortega Á., Nava M., Morillo D., Torres W., Hernández M., Cabrera M., Angarita L., Ortiz R., (2021) Advanced Glycation End Products: New Clinical and Molecular Perspectives. International Journal of Environmental Research and Public Health.; 18(14):7236.

21. Sen S., Kar M., Roy A., Chakraborti A.. (2005) Effect of nonenzymatic glycation on functional and structural properties of hemoglobin, Biophysical Chemistry, 113(3), 289-298,

22. Song Q ., Liu J., Dong L., Wang X., Zhang X., (2021) Novel advances in inhibiting advanced glycation end product formation using natural compounds, Biomedicine & Pharmacotherapy, 140, 111750

23. Shimasaki T., Yoshida H., Kamitori S., Sode K., (2017) X-ray structures of fructosyl peptide oxidases revealing residues responsible for gating oxygen access in the oxidative half reaction, Sci Rep, 7

24. Troester M., Lindstrom A., Kupper L., Waidyanatha S., Rappaport S., (2000) Stability of Hemoglobin and Albumin Adducts of Benzene Oxide and 1,4-Benzoquinone after Administration of Benzene to F344 Rats, Toxicological Sciences, 54(1), 88-94

25. Ulrich , P., Cerami, A. (2001). Protein glycation, diabetes, and aging. Recent progress in hormone research, 56(1), 1-22.

26. Vekic J., Vujcic S., Bufan B., Bojanin D. , Al-Hashmi K., Al-Rasadi K., Pantea Stoian A., Zeljkovic A., Rizzo M., (2023) The Role of Advanced Glycation End Products on Dyslipidemia, Metabolites, 13(1), 77

27. Verzijl N., DeGroot J., Thorpe S., Bank R., Shaw J., Lyons T., Bijlsma J., Lafeber F., Baynes J., TeKoppele J., (2000) Effect of Collagen Turnover on the Accumulation of Advanced Glycation End Products, Journal of Biological Chemistry, 275(15), 39027-39031

28. Vlassara H., Palace M.R., (2002) Diabetes and advanced glycation endproducts. Journal of Internal Medicine, 251, 87-101

29. Zeng C., Li Y., Ma J., Niu L., Tay F., (2019) Clinical/Translational Aspects of Advanced Glycation End-Products, Trends in endocrinology & metabolism, 30(12), 959-973.

Bakalaura darbs “Expression, purification and characterization of amadoriase mutants for the detection of glycated hemoglobin” izstrādāts LU Bioloģijas fakultātē

Ar savu parakstu apliecinu, ka pētījums veikts patstāvīgi, izmantoti tikai tajā norādītie informācijas avoti un LUISā iesniegtā darba elektroniskā kopija atbilst izdrukai un/vai e-studijās iesniegtai darba elektroniskai versijai.

Autors: Leonid Rozanov 30.05.2024

Rekomendēju darbu aizstāvēšanai

Dr. chem. Emilio Parisini 30.05.2024

Recenzents: Dr. biol. Kaspars Tārs

Darbs iesniegts LU Bioloģijas fakultātē 30.05.2024

Studiju metodiķe: ……

Darbs aizstāvēts Bioloģijas bakalaura gala pārbaudījuma komisijas sēdē

prot. Nr. , vērtējums

Komisijas sekretārs/e: